UNIVERSITY OF HELSINKI

Towards Molecularly Imprinted Polymers for Lignans: Isolation of Pinoresinol from Spruce Resins and Synthesis of Precursors

Master’s programme in Chemistry and molecular sciences
Master's thesis

Author:
Elli Ramu

Supervisor:
University Lecturer Norbert Maier

20.3.2025
Helsinki

Faculty: Faculty of Science
Degree programme: Master's programme in Chemistry and molecular sciences
Study track: Analytical chemistry
Author: Elli Ramu
Title: Towards Molecularly Imprinted Polymers for Lignans: Isolation of Pinoresinol from Spruce Resins and Synthesis of Precursors
Level: Master's thesis
Month and year: March 2025
Number of pages: 50
Keywords: Molecularly imprinted polymers, Pinoresinol, Norwegian spruce resin, Solid-phase extraction, High pressure liquid chromatography
Supervisor: University Lecturer Norbert Maier
Where deposited: E-thesis
Additional information:
Abstract:
The literature parts of this thesis review the methods for preparation, characterization and analytic applications of molecularly imprinted polymers (MIPs) for the isolation and enrichment of natural compounds from complex plant matrices.

Historically natural products have been extensively exploited for treatment of medicinal conditions and still represent a valuable source of new biologically and pharmaceutically active compounds. However, isolating bioactive compounds from plants is challenging due to the complexity of matrices and typically low concentrations. In context of this challenge, highly selective MIPs may greatly facilitate both enrichment and isolation. In contrast to biological affinity materials, such as antibodies and aptamers, MIPs are chemically robust, thermally stable, and readily re-usable.

The experimental section of this work reports the enrichment of biologically active lignan Pinoresinol from Norwegian spruce resin using multi-solvent sequential hot extraction followed by normal-phase column chromatography. In addition, various procedures for the preparation of precursors for the synthesis of Pinoresinol, i.e. coniferyl alcohol, 4-O-benzylvanillic alcohol, and 4-O-benzylvanillic acid, were explored. To facilitate these tasks, a validated HPLC-UV method for the quantitation of 4-O-benzylvanillic acid and 4-O-benzylvanillic alcohol. The method was determined to be repeatable and well fit for the analyte quantification was developed. The results of this research are expected to facilitate preparative scale access to Pinoresinol for future projects dedicated to the preparation of target-specific MIPs.

Table of contents

List of Abbreviations and Symbols Used 5

1 Introduction 7

2 Literature review on molecularly imprinted polymers in plant compound extraction 9

2.1 Molecularly imprinted polymers 9

2.2 Parameters evaluation of molecularly imprinted polymer function 11

2.3 Polymerization mechanism in molecularly imprinted polymer synthesis 13

2.4 Methods for molecularly imprinted polymer production 16

2.5 Morphological and chemical evaluation of molecularly imprinted polymers 18

2.6 Molecularly imprinted polymers in plant active compound separation 19

2.7 Conclusions and discussion of literature 22

3 Experimental work 23

3.1 Introduction 23

3.2 Materials and Instrumentation 27

3.3 Experimental methods 29

3.3.1 Resin extraction and column chromatography of extracts 29

3.3.2 Cannizzaro reaction 33

3.3.3 Pinoresinol **1** precursors from ferulic acid **6** 38

3.4 Results of experimental work 41

3.4.1 Resin Extraction and Column Chromatography 41

3.4.2 Calibration method for Cannizzaro reaction analysis 42

3.4.3 Yields and product purities of the Cannizzaro reactions 43

3.4.4 4-Acetoxyferulic acid **7,** 4-Acetylferuloyl chloride **8**, and 4-Acetoxylconiferyl alcohol **9** 44

3.5 Conclusions and discussion of experimental work 46

References 48

Appendices 51

Appendix 1. Overlaid chromatograms from multi-solvent sequential hot extraction, with Pinoresinol 1 marked with a black arrow. 51

Appendix 2. Calibration method LOD and LOQ values for all measured wavelengths 52

Appendix 3. Example of overlaid chromatograms (230 nm) of one calibration series. 52

Appendix 4. Example of a calibration series peak areas fitted against injected mass with the regression analysis 53

Appendix 5. Chromatograms (230 nm) of the Cannizzaro products from homogeneous and heterogeneous reaction conditions 54

Appendix 6. Chromatographs of crude and recrystallized 4-Acetoxyferulic acid and the mother liquor of the recrystallization 55

Appendix 7. Overlaid chromatograms of the reduction of 4-Acetylferuloyl chloride 12 (red arrow) to produce 4-Acetoxylconiferyl alcohol 13 (black arrow). 56

List of Abbreviations and Symbols Used

4-O-benzylvanillic aldehyde	BMB-Al
4-O-benzylvanillic alcohol	BMB-OH
4-O-benzylvanillic acid	BMB-A
A coordinated halide ligand	$X\text{-}M^{n+1}/L$
Absorbent capacity	Q
Acetonitrile	ACN
Alkyl halide	R-X
Atom transfer radical polymerization	ATPR
Azobisisobutyronitrile	AIBN
Binding affinity	K_a
Bound target concentration	C_{tb}
Column chromatography	CC
Ethyl acetate	EA
Ethylene glycol di-methacrylate	EGDMA
Formic acid	FA
Free radical polymerization	FRP
Free target concentration	C_{tf}
Imprinting factor	IF
Ligand-coordinated transition metal complex	M^n/L
Limit of detection	LOD
Limit of quantitation	LOQ
Living radical polymerization	LRP
Magnetic molecularly imprinted polymer	MMIP
Mass	m
Maximum absorption capacity	Q_{max}
Methacrylic acid	MAA
Micro column chromatography	mCC
Molecularly imprinted polymer	MIP
n-Hexane	HEX
Nitroxide-mediated polymerization	NMP
Non-imprinted polymer	NIP
Polystyrene	PS
Propagating polymer	$P_n\bullet$ and $P_m\bullet$
Radical	R•
Rate of deactivation	k_{deact}
Rate of initiation	k_i
Rate of propagation	k_p
Rate of termination	k_t
Rate of activation	k_{act}
Relative selectivity coefficient	k'
Reversible addition-fragmentation chain transfer	RAFT
Scanning electron microscopy	SEM
Selectivity coefficient	k
Selectivity	α
Signal to noise ratio	S/N
Surface molecular imprinting technique	SMIT

Tert-butyl methyl ether	tBME
Transmission electron microscopy	TEM
Vinyl pyridine	VP
Volume	V

1 Introduction

Before the advent of modern synthetic drug production, for millennia humans have relied on natural products for the treatment of a wide range of diseases.[1,2] For example in Nordic countries, especially in Finnish Lapland, ointment prepared from the Norwegian spruce (*Picea abies*) resin has been used for centuries to treat acutely and chronically infected injuries.[3] Medicinal plants typically contain a large variety of bioactive compounds at relatively low concentrations and is a primary source for the discovery of new drug candidates.[2,4] However, the matrix complexity of plant materials renders the enrichment and isolation of these valuable compounds difficult.[4] Common preparative and analytical isolation methods rely on liquid-liquid extraction,[5] column chromatography,[6] and thin-layer chromatography.[7] Unfortunately, these methods are often labor and solvent-intensive, rendering them poor choices in terms of sustainability and associated costs. In this context the processes utilizing target specific affinity materials for compound isolation appear attractive. In particular, Molecularly Imprinted Polymers (MIPs) are a class of synthetic polymers engineered to exhibit antibody-like specificity toward a target molecule.[4,8] These polymers are highly selective,[8] reusable,[9] and potentially more sustainable than traditional solvent-intensive or single-use separation methods,[8,9] making them valuable for a wide range of applications, including compound separation from plant biomass.[8]

The following literature review focuses on the function, synthesis, and application of MIPs in the separation of compounds from plant biomass. It provides an overview of the fundamentals of MIP function, commonly used polymerization methods and imprinting techniques, evaluation strategies for MIP performance, and literature examples of MIP-based compound separation from plant materials. While the applications of MIPs are of broad scope,[8–11] this review covers preferentially applications in context with isolation and enrichment of important natural compounds from plant materials.

The focus of the literature review has particular relevance for the experimental section of this thesis, which focuses on the enrichment of Pinoresinol, from Norwegian spruce (*Picea abies*) resin. Pinoresinol is a lignan metabolite providing a broad spectrum of favorable biological activities, and also defense against environmental stressors.[12] The experimental work of this thesis perused two main goals. The first goal was to enrich Pinoresinol form *Picea abies* resin using a combination of multi-solvent sequential hot extraction and column

chromatography. The second goal was to test protocols for the synthesis of various Pinoresinol precursors, i.e., coniferyl alcohol,[13,14] 4-O-benzylvanillic acid, and 4-O-benzylvanillic alcohol,[15,16] and develop analytical methods for comparative evaluation the performance of these synthesis protocols.

2 Literature review on molecularly imprinted polymers in plant compound extraction

2.1 Molecularly imprinted polymers

Molecularly imprinted polymers (MIPs) are a class of polymers that mimic natural antibodies. MIPs display molecular recognition cavities for the specific binding of target molecules. These cavities are obtained by templated polymerization in presence of the target molecules, generating sites that match the three-dimensional shape and functionalities of the employed templates. Often, these polymer-embedded display binding specificities and affinities similar to those seen for antigen-antibody interactions.[4,8] The main advantages of MIPs over biological affinity materials are high selectivity, relatively simple preparation methods, reusability, relatively low cost of synthesis materials, and long-term stability.[9,17–19] Especially the reusability and stability of MIPs make them potentially more cost-effective and sustainable compared to single-use methods, such as biological antibodies. However, MIP synthesis and optimization often requires weeks of trial and error experimentation.[9] In addition, MIP synthesis always requires a template molecule, i.e. the target molecule or a close structural analog.[4,8,9,20] However, acquiring sufficient amounts of a given template for the MIP synthesis can be costly and time-consuming, posing some limits in applications.[9]

Conventional MIP synthesis is based on radical polymerization. MIP synthesis generally requires pre-polymerization mixtures consisting of the template, a functional monomer, a cross-linker, an initiator, and a porogenic solvent. (Figure 1, part 1).[4] In this stage, the template interacts with the functional monomers, which preform the functional group repertoire of the binding sites. Functional monomers can interact with the templates either through covalent bonding or non-covalent interactions. In the case of non-covalent molecular imprinting, the interactions of the template with monomers is restricted to non-covalent interactions (van der Waals forces, hydrogen bonding, ionic interactions).[9] In the covalent imprinting approach, the functional monomers are covalently attached to the template.[4,21] The template plays a crucial role in shaping the polymer's binding cavities.[20] Chemical inertness and solubility in the pre-polymerization mixture are essential requirements for templates for molecular imprinting.[22] In the polymerization stage, the monomers form polymer chains via cross-linkers to form the walls of the recognition cavities around the templates (Figure 1, part 2).[4,21] The level of cross-linking controls the polymer morphology and

swellability, with high levels stabilizing the imprinted binding sites and providing favourable mechanical stability. Low levels of cross-linking leads to poor mechanical stability, while exceedingly high levels reduce the number of recognition sites.[22] Several type of distinct polymerization reactions can be used for molecular imprinting,[4] which shall be treated in detail later (Section 2.3.). The final stage of MIP production is the elution of the template (Figure 1, part 3). If the template is covalently bound to the imprinted polymeric matrix, these covalent bonds need to be cleaved using appropriate chemistries. In the case of non-covalent imprinting, the template molecules can simply be extracted from the cavity with an appropriate solvent.[23] The elution of the template leaves behind a cavity with active sites capable of rebinding to the template molecule.[4]

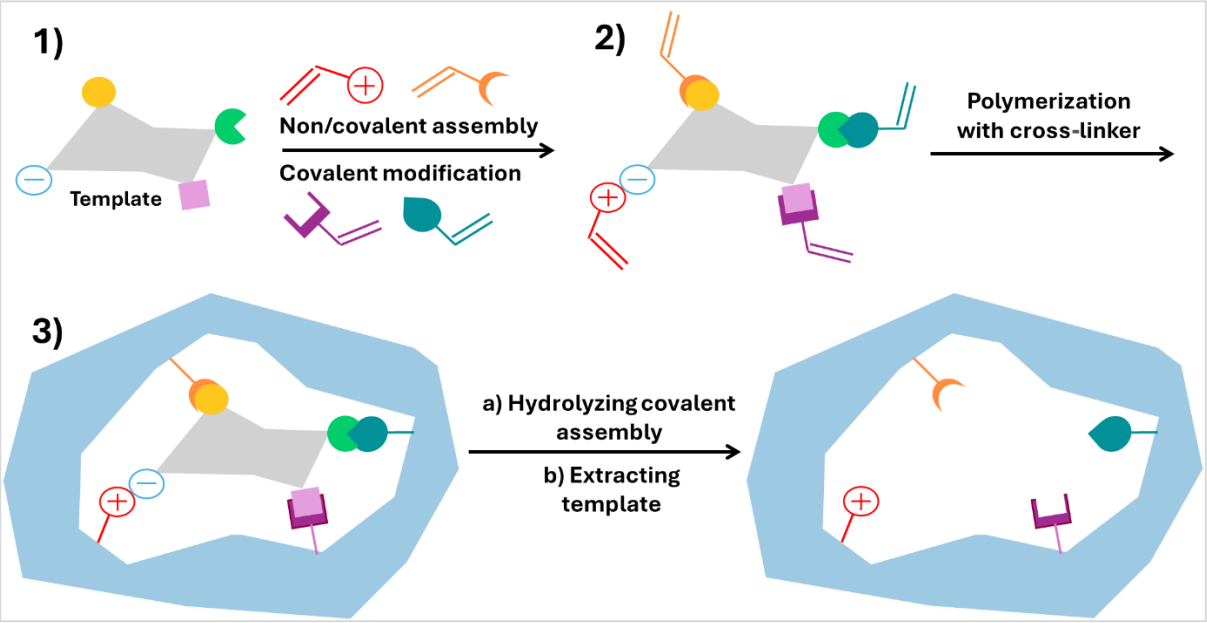

Figure 1. Schematic presentation of conventional MIP synthesis steps: 1) The pre-polymerization stage, 2) polymerization stage, 3) Removal of template. Figure was drawn based on Zuo et al. (2023)[4].

Examples of covalent and non-covalent imprinting can be seen in Figure 2.

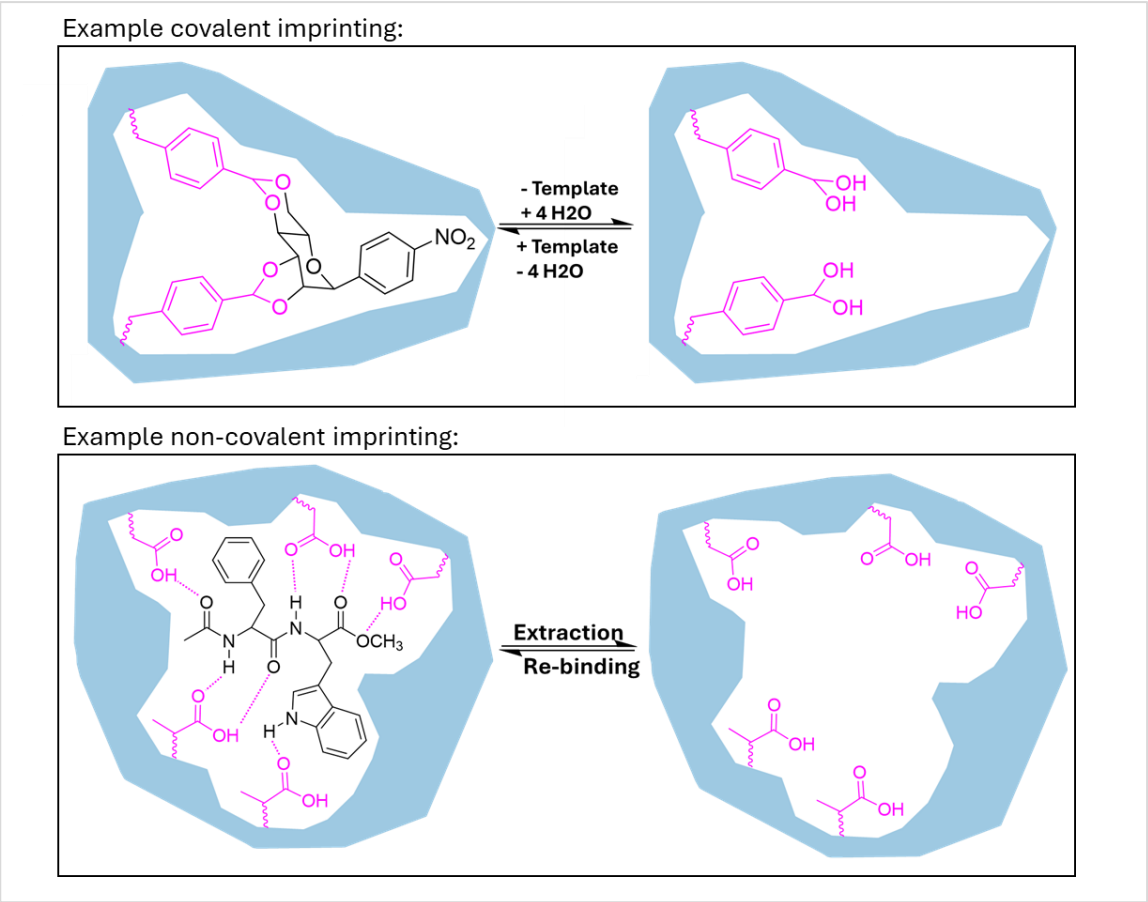

Figure 2. Example covalent imprinting of -nitrophenyl-α-d-mannopyranoside-2,3:4,6-di-O-(4-vinylphenylboronate) and non-covalent imprinting of a dipeptide derivative (methyl acetylphenylalanyltryptophanate). Figure was drawn based on Maier and Lindner (2007)[23].

2.2 Parameters evaluation of molecularly imprinted polymer function

Many parameters exist for evaluating MIPs and the success of MIP synthesis. These parameters are frequently used in the literature to evaluate how a MIP performs in the separation of the selected target analyte. Many of them are also referred to in this work.

The adsorption capacity (Q) describes the amount of analyte the MIP can absorb per mass of MIP. Q can be described with the equation

$$Q = \frac{C_0 - C_1}{m}, \quad (1)^{4,10,24}$$

where C_0 is the original concentration of the target analyte, C_1 is the analyte concentration after adsorption equilibrium is reached, and m is the MIPs mass.[4,24] The distribution coefficient (K_d) can also be used to measure the efficiency of the MIP according to equation

$$K_d = \frac{(C_0 - C_1)V}{mC_1}, \quad (2)^{4,10,24}$$

where V is the volume of the solution.

The success of the imprinting process can be determined using the Imprinting Factor (*IF*) and selectivity (α).[10,24] *IF* is calculated using the equation

$$IF = \frac{Q_{MIP}}{Q_{NIP}}, \quad (3)[24]$$

where Q_{MIP} is the adsorption capacity of the MIP, and Q_{NIP} is the adsorption capacity of a control polymer called Non-Imprinted Polymer (NIP).[24] The NIP is synthesized with the same method as the corresponding MIP, but without the template.[10] For α, the Q and *IF* values of the analyte and a structurally similar analog can be used to form equations

$$a = \frac{Q_{analyte}}{Q_{analog}}, \quad (4)[10]$$

and

$$a = \frac{IF_{analyte}}{IF_{analog}}. \quad (5)[10]$$

The binding interactions between the imprinted polymer and the target molecule can be described with a Scatchard Plot. This plot helps to determine the binding affinity (K_a) and heterogeneity of binding sites. The Scatchard Plot follows equation

$$\frac{C_{tb}}{C_{tf}} = K_a(Q_{max} - C_{tb}) \quad (6)[25]$$

where C_{tb} is the concentration of the bound target molecule, C_{tf} is the concentration of the free target molecule, K_a is the binding affinity, and Q_{max} is the maximum binding capacity.[26] The Scatchard Plot can be linear or curved. A linear Scatchard Plot indicates a single class of binding sites with uniform affinity, while a downward-curved plot indicates the presence of both high-affinity and low-affinity binding sites. The Scatchard Plot can also have multiple linear regions, which suggests at least two distinct binding sites with different affinities.[25]

Selectivity coefficient (k) and relative selectivity coefficient (k') can also be used to evaluate the selectivity of a MIP. Using the K_d values of the target analyte and a structural analog, k can be calculated according to equation

$$k = \frac{k_{analyte}}{k_{analog}} \quad (7)[10,24]$$

for both the MIP and NIP.

With the calculated k_{MIP} and k_{NIP} values the k' can be calculated according to equation:

$$k' = \frac{k_{MIP}}{k_{NIP}} \quad (8)^{10,24}$$

2.3 Polymerization mechanism in molecularly imprinted polymer synthesis

Several radical polymerization methods are in use for MIP synthesis. This section describes commonly used Free Radical Polymerization (FRP) and Living Radical Polymerization (LRP) methods described in the literature.

FRP is a well-established and the most simple method for MIP synthesis.[4,27] In FRP, the polymer is formed through the successive additions of free-radical monomers. FRP involves three main stages: initiation, propagation, and termination. During initiation, free radicals are generated, typically through the decomposition of an initiator. The formed free radicals then react with monomers to form reactive centers. In the propagation step, these reactive centers add to monomer molecules successively, forming a growing polymer chain. Finally, termination occurs through recombination or disproportionation of free radicals, which stops the polymer growth.[28] In FRP, the concentration of free radicals is relatively high which leads to uncontrollable propagation and termination of the reaction.[4] The uncontrollability of the reaction gives rise to heterogeneity within the formed polymer network and leads to a loss of template binding capacity and affinity of the MIPs.[29,30] Other synthesis methods have been developed to increase the template binding and decrease the binding site heterogeneity.[29] The reaction mechanism of FRP is depicted in Figure 3, where $R^{\cdot}$ is a free radical, k_i is the reaction rate of the initiation, k_p is the rate of the propagation, and k_t is the rate of the termination reaction.

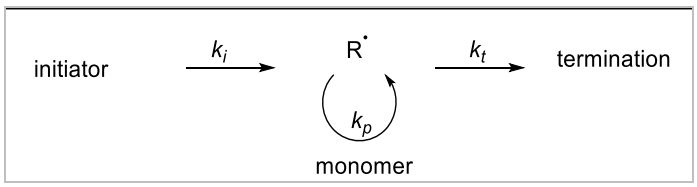

Figure 3. General reaction mechanism of FRP.[16]

Living Radical Polymerization (LRP) is a form of controlled chain growth polymerization where the polymer chains grow through a persistent, active free radical at the chain end. Unlike FRP, LRP enables precise control over the polymerization process.[31] The key advantage of LRP is the suppression of chain termination reactions, allowing for better control over the polymer's molecular weight, distribution, and architecture.[32] There are three main methods in LRP: Atom Transfer Radical Polymerization (ATRP),[33] Reversible Addition-Fragmentation Chain Transfer (RAFT) Polymerization,[33,34] and Nitroxide-Mediated Polymerization (NMP).[35]

In ATRP the polymerization reaction is initiated with an alkyl halide (R-X), catalyzed typically by a ligand-coordinated transition metal complex (M^n/L). Transition metals, such as copper, iron, ruthenium, nickel, and osmium, are commonly used. During the ATRP process, the alkyl halide species is activated by the transition metal complex, generating radicals through a one-electron transfer mechanism. This interaction generates propagating radicals and the metal complex in its higher oxidation state with a coordinated halide ligand (e.g. X-M^{n+1}/L). The activation of radicals occurs with a measurable rate constant k_{act}, followed by propagation with k_p. The activation reaction is reversible both for the initially formed radical and the growing polymer chain. The reversible deactivation of the radicals has the rate constant k_{deact}. As ATRP is a radical-based process, termination can still occur with the rate constant k_t. The dominant reaction equilibrium in ATRP is between the activation and deactivation of the growing polymer chain (P_n•) with the deactivation of the chain being a dominant reaction direction. This balance decreases the termination reactions of the polymer chain, making the ATRP reaction controllable by the concentration of the catalyst.[33] ATRP activation and main equilibrium mechanisms can be seen in Figure *4*.

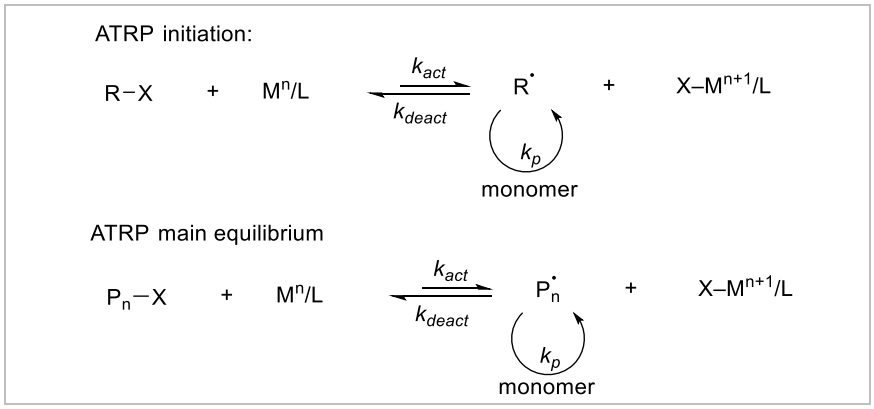

Figure 4. The general mechanism for ATRP initiation and main equilibrium.[33] The initiation steps and terminations have been left out of the figure for improved readability.

In RAFT, the control over the product polymer's molecular weight is achieved, similarly to ATRP, through a reversible activation-deactivation equilibrium of the polymer chain. Radicals are generated similarly to FRP with an initiator. The initiator decomposes to form radicals that react with monomer molecules, producing propagating radicals ($P_m^{\bullet}$). After the initiation step, the $P_m^{\bullet}$ adds to a C=S bond of a Chain Transfer Agent and enters an equilibrium between active and dormant state of the polymer.[34] The Chain Transfer Agent is generally a thiocarbonylthio group Z–C(=S)S–R where Z and R are substituents.[36] This addition is reversible and it generates an intermediate radical which temporarily stabilizes chain propagation. The intermediate radical reversibly fragments to form a new radical, which also propagates with monomers to form a new propagating polymer $P_n^{\bullet}$. A rapid reversible equilibrium forms between both growing radicals $P_n^{\bullet}$, $P_m^{\bullet}$, and the Chain Transfer Agent. This equilibrium is the main equilibrium of RAFT. As a result, the chains grow at a similar rate, and the polymerization can be stopped and restarted without loss of control. Without the Chain Transfer Agent, uncontrolled radical polymerization would result in a wide molecular weight range due to random termination events.[33,34] The RAFT pre-equilibrium and main equilibrium are shown in Figure 5.

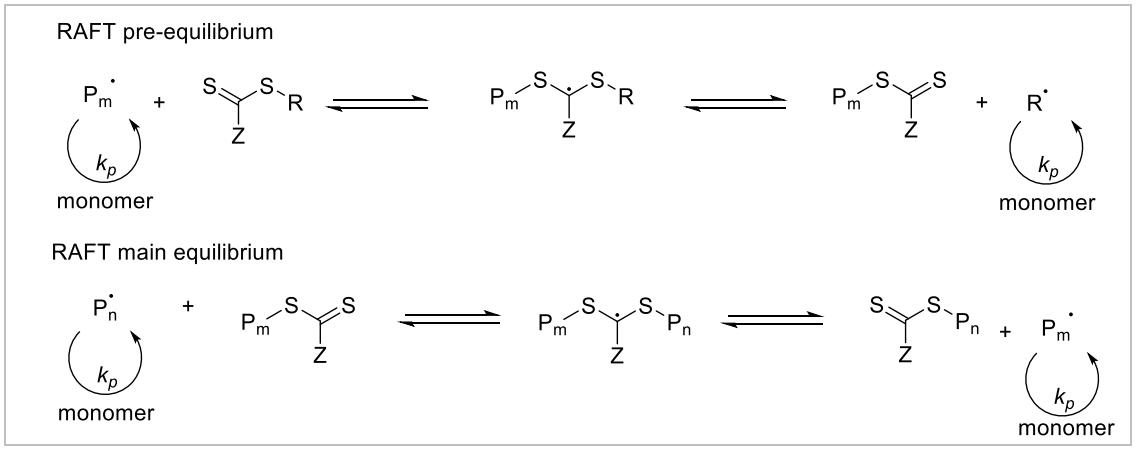

Figure 5. Pre-equilibrium and main equilibrium for RAFT.[33,34] The initiation steps and terminations have been left out of the figure for improved readability.

NMP is a radical polymerization method controlled by the presence of a nitroxide radical. The nitroxide reversibly deactivates the propagating chain $P_n^{\bullet}$, forming a dormant species. This equilibrium between active and dormant states minimizes uncontrolled chain growth and termination reactions.[35] The general mechanism for the NMP equilibrium can be seen in Figure 6.

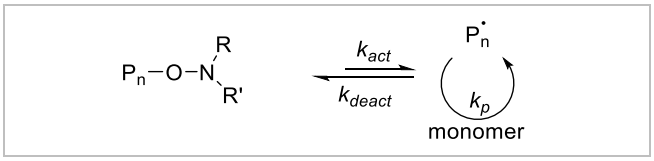

Figure 6. The reaction mechanism for NMP.[35] The initiation steps and terminations have been left out of the figure for improved readability.

2.4 Methods for molecularly imprinted polymer production

A variety of preparation methods have been developed for MIP production. The most commonly used methods include bulk polymerization[37,38], suspension polymerization,[39,40] precipitation polymerization,[41] surface molecularly imprinting technique (SMIT)[42,43], emulsion polymerization, and dummy molecularly imprinting.[4,20,44,45] Variants of emulsion polymerization exist for the synthesizing MIP micro and nanoparticles.[46,47] Dummy molecular imprinting describes the use of a template molecule that is structurally similar to the target analyte. The target analyte can be unsuitable as a template due to instability in polymerization conditions, high price, or poor availability. In addition to addressing template unsuitability, dummy imprinting also helps mitigate potential issues with residual template bleeding into samples during the MIP's post-synthesis use.[4,9,20,40]

Bulk polymerization is the most conventional and simple method for MIP synthesis.[38] The general procedure of bulk polymerization starts with dissolving monomer molecules to a solvent, followed by cross-linking agents and initiators. The formed solution is purged of oxygen using nitrogen gas followed by the initiation by photoionization or thermal initiation. The following polymerization results in a block of polymer, that can be ground down to particles of the desired size.[48,49] Bulk polymerization often leads to poor adsorption capacity of the target molecules due to covered binding cavities and difficulty in removing the templates. The particle size achieved with grinding is often irregular, and grinding leads to the destruction of binding sites.[4,50]

Precipitation polymerization is similar to bulk polymerization, in that all components needed are soluble in the used solvent. A large amount of solvent is used to dissolve the components, but the formed MIP is not soluble and will precipitate as the polymerization proceeds. Unlike bulk polymerization, precipitation polymerization does not require the grinding of the formed polymer. This leads to more intact binding cavities, and more uniform particle size distribution.[39]

Suspension polymerization is a heterogeneous polymerization method, where the monomers, oil-soluble initiators, and dispersant are dispersed in aqueous phase. Polymerization in this method happens in the dispersant droplets, resulting in the polymers forming as separate spheres in the solvent. Suspension polymerization leads to uniform particle size, more available binding cavities and does not require the binding cavities destroying from grinding[4,39] In addition, the use of water as the polymerization medium instead of organic solvents is a notable benefit of suspension polymerization. Water has many advantages as a solvent, including easy accessibility, low cost, non-toxicity, renewability, and the ease of wastewater treatment.[41]

SMIT is a novel method developed to solve the common issues binding site unavailability issues with conventional MIP synthesis methods.[43] In SMIT, the polymerization is conducted on the surface of a solid carrier particle in the presence of the templates, initiators, and cross-linking agents. The resulting MIPs' binding cavities are on the surface of the polymer layer, or close to the surface. This makes the washing of templates and re-adsorbing target analytes easy with SMIT-produced MIPs. Compared to the more conventional polymerization methods, surface imprinted method produces more effective binding sites, and total surface area of the polymer per unit mass.[42,43]

Emulsion polymerization takes place in an aqueous medium, where water-insoluble monomers are emulsified with surfactants to form small droplets or micelles, typically yielding uniform polymer particles.[51] Mini-emulsion polymerization and core–shell emulsion polymerization are common methods for the production of micro- and nanoscale MIP particles.[10,39,46,52] Mini-emulsion polymerization involves a high-shear homogenization step and the use of a co-surfactant to achieve well-dispersed monomer droplets in an aqueous phase. The process typically starts with a high-energy input, such as ultrasound or mechanical stirring, breaking down monomer droplets into nanoscale sizes, ensuring

uniformity. A stabilizing agent prevents droplet merging, allowing controlled polymerization within each droplet. The monomer droplets act as individual nanoreactors where polymerization occurs, leading to the formation of stable nanoparticles within the size range of 50–500 nm. This method provides control over particle size and enhances reproducibility, making it suitable for large-scale applications.[46] Core–shell emulsion polymerization is a two-stage process for producing hybrid MIP nanoparticles, involving seed latex formation (0.03–1 μm) followed by the creation of an imprinted shell via emulsion polymerization. Core–shell emulsion polymerization offers high yields and improved rebinding capacity due to available sites from surface imprinting. However, surfactants and aqueous phases pose challenges in standardizing particle size and imprinting efficiency.[47] If the imprinted particle is magnetic, this method produces magnetic MIPS (MMIPs). MMIPs allow for rapid separation using an external magnetic field, eliminating the need for filtration or centrifugation.[10,39,52]

2.5 Morphological and chemical evaluation of molecularly imprinted polymers

In addition to the parameters provided in Chapter 2.2, knowledge of the morphology of the synthesized MIPs can be used to assess synthesis success.[53] The physical properties of MIP particles, such as shape, size, and surface functionalization, significantly impact the performance of MIPs. Uniformly shaped MIPs with available binding cavities are more effective for target analyte adsorption.[54] Various analytical techniques exist for characterizing MIP morphology, providing insight into surface and internal structure, porosity, and polymer uniformity.

The resolution of optical microscopes is limited by the wavelength of light to approximately 200-300 nm,[55] making them unsuitable for the analysis of nanoparticles.[53] Transmission Electron Microscopy (TEM) and Scanning Electron Microscopy (SEM) are good options for nanoscale imaging. TEM is used to analyze internal structures by transmitting electrons through a sample,[20,53] while SEM scans surfaces, providing high-resolution images and compositional information.[53] TEM and SEM images are often used to determine particle size and possible cavities in MIP particles.[18,20,40,56]

Brunauer-Emmett-Teller analysis is a method used to measure the surface area, pore size, and pore volume of MIPs.[57] This technique is crucial for understanding the porosity of the polymer, which influences the binding capacity of the MIP.[4] The Brunauer-Emmett-Teller analysis method determines total surface area by measuring the adsorption of chemically inert gases, like helium or nitrogen, on pores and flat surfaces. Since the Brunauer-Emmett-Teller analysis does not rely on pore filling, particle and pore morphology have little influence on the results.[58]

Beyond morphological analysis, Fourier Transform Infrared spectroscopy is used to identify functional groups present in MIPs, compare MIP and NIP structures,[20,59] and confirm template removal.[60] Fourier Transform Infrared spectroscopy is a widely employed analytical method in MIP research that characterizes molecular identity through the detection of vibrational and rotational transitions. By measuring the absorption of infrared radiation at wavelengths corresponding to changes in a molecule's dipole moment, it generates unique spectral profiles reflective of a substance's atomic composition and structural configuration.[59,61]

2.6 Molecularly imprinted polymers in plant active compound separation

MIPs can be used as a solid-phase adsorbent for separating compounds from complex mixtures.[18,20,40,52,62,63] The antigen-antibody-like selectivity of MIPs allows them to separate compound groups even from complex mixtures.[62] A literature survey was conducted to provide examples of MIP applications in plant compound separation. A collection of the found use cases can be seen in Table 1. The table lists the target plant, template, crosslinker, initiator, and the Q and IF values (Equations (1) and (3)), if available. For a more comprehensive review of the latest MIP application in plant compound separation, see the review article by Zuo et al. (2023)[4].

The literature survey identified numerous MIP-based methodologies for separating flavonoids,[64–70] glycosides,[20,37,71] other polyphenols,[17,18,72] terpenoids,[57,73,74] and coumarins[75–77] from diverse plant sources. As shown in Table 1, a variety of functional monomers have been used in MIP research, with vinylpyridine (VP), methacrylic acid (MAA), and various acrylamides being the most prevalent. Additionally, unconventional monomers, such as the small protein lysozyme were reported,[18] demonstrating comparable separation efficiencies based on the provided *Q* and IF values (Equations (1) and (3)). Ethylene glycol dimethacrylate (EGDMA) was identified as the most commonly utilized crosslinker, while azobisisobutyronitrile (AIBN) predominated as the initiator. The majority of the surveyed studies involved imprinting on particles, encompassing both magnetic particles, such as Fe_3O_4, and non-magnetic particles, like polystyrene (PS).

The most common motivation in the reviewed studies is the separation of compounds with potential health benefits or medicinal applications. Examples include luteolin, quercetin, coumarins, and hesperetin, all of which exhibit anti-inflammatory properties.[65,66,69,76] However, non-health-related applications were also documented. For instance, the separation of limonin from lemon juice was pursued to reduce bitterness and enhance palatability.[74]

Table 1. Survey of MIP applications in different plant compound separations. Table includes the target plant, template, carrier, functional monomer, crosslinker and initiator, and the IF and Q values, if provided.

	Template	Plant	Carrier	Functional monomer	Crosslinker	Initiator	Parameters	Ref
Flavonoids	Luteolin	Peanut shell	SnO_2	4-Vinylphenylboronic acid, MAA	Catechol	AIBN	*Q*: 16.55 mg/g	65
	Quercetin	Onion samples	Fe3O4@-SiO2@NH2	MAA	EGDMA	AIBN	*Q:* 85.5 mg/g	66
	Dihydro-quercetin	*Larix griffithiana*	NH_2-SiO_2@ Fe_3O_4	2-VP	EGDMA	AIBN	-	67
	Proantho-cyanidin	Camelli seed shells	chitosan	acrylamide	trimethylol-propane	AIBN	*Q*: 6.8 mg/g	68
	Hesperetin	*Citrus reticulata blanco*	Fe_3O_4	N-isopropyl-acrylamide	EGDMA	AIBN	Q: 31.4 mg/g	69
	Myricetin	*Carthamus tinctorius* l.	–	4-VP glycidyl methacrylate	EGDMA	AIBN	*Q*: 10.6 mg/g	70
	Farrerol Dummy: Quercetin	*Rhododendron aganniphum*	–	4-VP	EGDMA	AIBN	*Q*: 20.7 mg/g IF: 3.10	64
Glycosides	Acteoside	*Cistanche tubulosa*	–	4-VP	EGDMA	AIBN	*Q*: 168.1 mg/g IF: 2.69	37
	Rutin and Rutinoside	Green tea	Fe_3O_4	MAA, 4-VP	Divinylbenzene	AIBN	IF*:* 3.4 and 66.5	71
	D-Glucose	Soy	PS	3-aminophenylboronic acid	EGDMA	AIBN	*Q:* 33-35 µg/g IF: 2.5-2.9	20
Other polyphenols	Chlorogenic Acid	*Honeysuckle*	Fe_3O_4-Cu	Lysozyme	-	-	*Q*: 10.8 mg/g IF: 2.86	18
	Chlorogenic Acid	Duzhong brick tea	SiO_2	4-VP	EGDMA	AIBN	*Q*: 42.2 mg/g	17
	Polydatin	Polygoni cuspidati rhizoma et radix	–	4-VP	EGDMA	AIBN	*Q*: 65 mg/g IF: 1.48	72
Terpenoids	Ginsenosides	*Panax ginseng*	Fe_3O_4	-	Catechol	poly(ethy-lene-co-vinyl alcohol)	*Q*: 0.8 mg/g IF: 3.7	73
	Limonin	Lemon juice	SiO_2	MAA	EGDMA	AIBN	*Q*: 27.7 mg/g IF: 4.33	74
	Andro-grapholide	Andrographis paniculata	–	3-Aminopropyl-triethoxysilane	Tetraethyl orthosilicate	acetic acid	IF: 1.22	57
Coumarisns	7-Hydroxy-Coumarin	Asafoetida	–	4-VP	EGDMA	AIBN	IF: 2.4	76
	Coumarins	Cinnamon, Chamomile Tea, and Wine	–	MAA, 4-VP	EGDMA	AIBN	-	77
	Dicoumarol	*Melilotus officinalis* l.	–	MAA	EGDMA	AIBN	*Q*: 0.045 mg/g	75

2.7 Conclusions and discussion of literature

MIPs are highly selective synthetic polymers that mimic natural antibody recognition,[8] enabling efficient enrichment and isolation of target compounds from complex plant matrices. Their high specificity, in combination with ease of preparation, chemical stability, broad organic solvent combability and re-useability, makes them particularly valuable tools for isolating plant-derived medicinal compounds.[18,37] The current literature shows that there is considerable interest in expanding the applications of MIPs for isolation separation of compounds with potential health-promoting properties.[4] In terms of analytical applications, MIPs are primarily employed for solid phase applications in packed column formats to isolate specific target molecules from crude plant extracts. Common target molecules in the literature included flavonoids, glycosides, other polyphenols, terpenoids, and coumarins. However, the development of MIPs with highly selective binding properties remains challenging and often requires considerable experimental efforts to match the complex interplay relies of template, functional monomers, cross-linkers, initiators, and porogenic solvents, and the appropriate polymerization conditions.

It is worth mentioning that various polymerization techniques can be employed in the synthesis of MIPs to control both general polymer properties and morphology. While operationally simple methods FRP and bulk polymerization may deliver MIPs low binding density and poor stability, more sophisticated LRP polymerization techniques offer more convenient control over polymer morphology, allowing preparation of supported MIPs, such as magnetic particle formats.

3 Experimental work

3.1 Introduction

Pinoresinol **1** (Figure 7 A)) is a tetrahydrofuran lignan.[3,12] Lignans are a subgroup of polyphenols, and a major group of secondary metabolites widely present in the plant kingdom.[12] Polyphenols are produced by plants for protection against environmental threats, such as UV radiation and parasites.[78] In addition to Norwegian spruce (*Picea abies*), Pinoresinol **1** is found in several plants, such as olives (*Olea europaea*),[79] sesame (*Sesamum indicum*),[13,80] and North China Red Elder (*Sambucus williamsii*).[81] The Pinoresinol **1** content of *Picea abies* resin is approximately 12 m-%.[82]

Due to the antifungal effects of Pinoresinol **1** and existing use cases of spruce resin in medicine,[3,83] we were interested in finding methods, to selectively separate Pinoresinol **1** from resin. We were especially interested in MIPs as a separation medium in future research efforts, to which Pinoresinol **1** standards are needed. Due to the need for Pinoresinol **1** standards, the first goal of this experimental work was to separate Pinoresinol **1** from resin using multi-solvent sequential hot extraction and column chromatography (CC). The goal was to see how much Pinoresinol **1** could be separated using these methods and if pure Pinoresinol **1** standard could be acquired. The chosen solvents included n-hexane (low polarity), tert-butyl methyl ether (tBME) and ethyl acetate (EA) (medium polarity), and methanol (MeOH) (high polarity). Low polarity solvents were employed initially to reduce the number of impurities co-extracted with Pinoresinol **1**, while high polarity solvents were used at the end of the extraction process to recover any residual Pinoresinol **1** remaining in the resin. To identify the solvent that extracted the most Pinoresinol **1,** we used HPLC-UV/VIS. Micro column chromatography (mCC) was used as a preliminary screening technique to identify suitable solvent compositions for the enrichment of Pinoresinol **1** from the Pinoresinol **1**-containing extract. Silica gel 60 was used as the solid phase, because it has been used in literature for the separation of lignans in normal phase chromatography.[84,85] The mCC method involved pre-adsorbing extractables onto silica gel to prevent solubility issues and to enhance separation efficiency. Sequential elution was performed with increasing concentrations of EA in MeOH with acetic acid (AcOH) added for pH adjustment. Based on the findings from mCC, the method was scaled up 10-fold in sample amount in CC.

The second goal was the synthesis of Pinoresinol **1** precursors Coniferyl alcohol **2**, 4-O-benzylvanillic acid (BMB-A) **3,** 4-O-benzylvanillic alcohol (BMB-OH) **4** to enable future synthesis of Pinoresinol **1** standards for future MIP synthesis. Since Pinoresinol **1** separation from resin can be solvent-intensive, it would be beneficial to find synthesis pathways for Pinoresinol **1** for future MIP synthesis.

BMB-A **3** and BMB-OH **4** have potential in the synthesis of racemic Pinoresinol **1**.[15,16] Survey of the literature indicated that they could be conveniently accessed by an operationally simple Cannizzaro reaction (Figure 7 A)).[16] The Cannizzaro reaction is a synthesis method in organic chemistry, offering an efficient method for synthesizing alcohols and carboxylic acids from aldehydes. In the Cannizzaro reaction, two aldehyde molecules undergo simultaneous oxidation and reduction sequence in the presence of a strong base.[86] With the Cannizzaro approach, the BMB-A **3** and BMB-OH **4** could be synthesized using the corresponding aldehyde 4-O-benzylvanillic aldehyde (BMB-Al) **5** as seen in Figure 7 B). Singh et al. (2007)[16] described a one pot Cannizzaro reaction of 4 BMB-Al **5** using three molar equivalence of KOH in methanol solution and yielded 44% for the product BMB-A **3**, and 45% for the product BMB-OH **4**.[16] During previous efforts to reproduce the literature protocol at the 1.0 g substrate scale, it was observed that the reaction mixture reproducibly solidified at an early stage, rendering stirring and homogeneous heating of the reaction mixture elusive. Solidification of the reaction mixture within the reactor and the potential safety issues associated with this phenomenon was considered a serious limitation for the scaling to multiple gram amounts. For these reasons, this experimental work also studied the modification of the reported protocol, in which the reaction conditions were homogeneous. Homogeneity was achieved by increasing the volume of the solvent methanol (MeOH) in the reaction mixture. In addition, the HPLC-UV method was developed for the purpose of comparing the literature and modified Cannizzaro procedures. The goal of the method was to be able to quantify all three Cannizzaro products with satisfactory repeatability. Six independent calibration series were prepared, so that the repeatability of the method could be assessed. The Limit of Detection (LOD) and Limit of Quantification (LOQ) for all Cannizzaro compounds was also determined for the calibration methods, so that small peaks could be confidently analyzed.

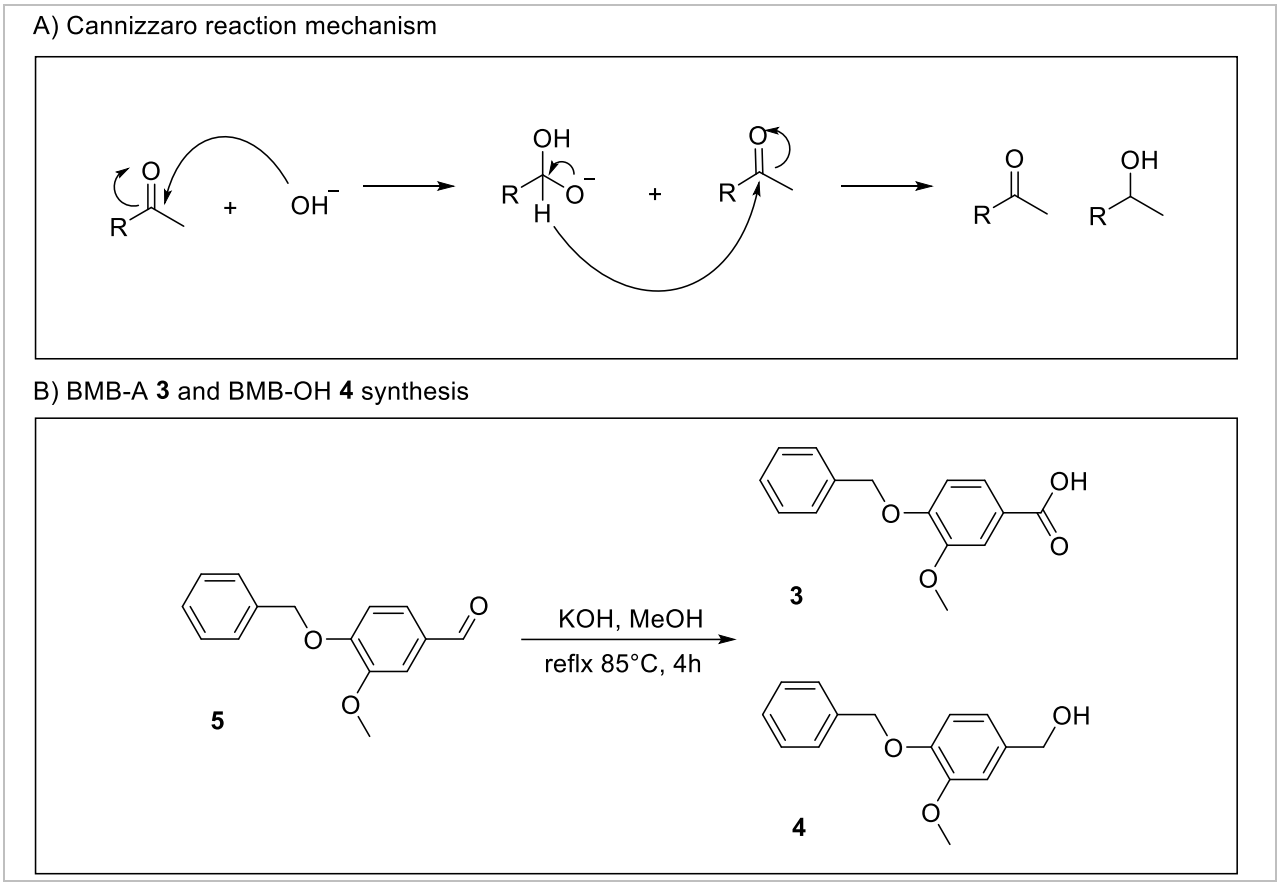

Figure 7. General mechanism of the Cannizzaro reaction.[86] B) Synthesis of BMB-A **3** and BMB-OH **4** through Cannizzaro reaction described by Singh et al. (2007)[16].

The synthesis pathway of Pinoresinol **1** from Coniferyl alcohol **2** includes two Coniferyl alcohol **2** molecules merging through radical coupling (Figure 8 A)). The radical coupling reaction is catalyzed by an oxidant, such as peroxidase.[13] We studied the multi-step synthesis pathways reported by Panzella et al. (2018)[87] and Hosoda et al. (2001)[88] for the synthesis of Coniferyl alcohol **2** from Ferulic acid **6.** The studied reaction scheme can be seen in Figure 8 B).

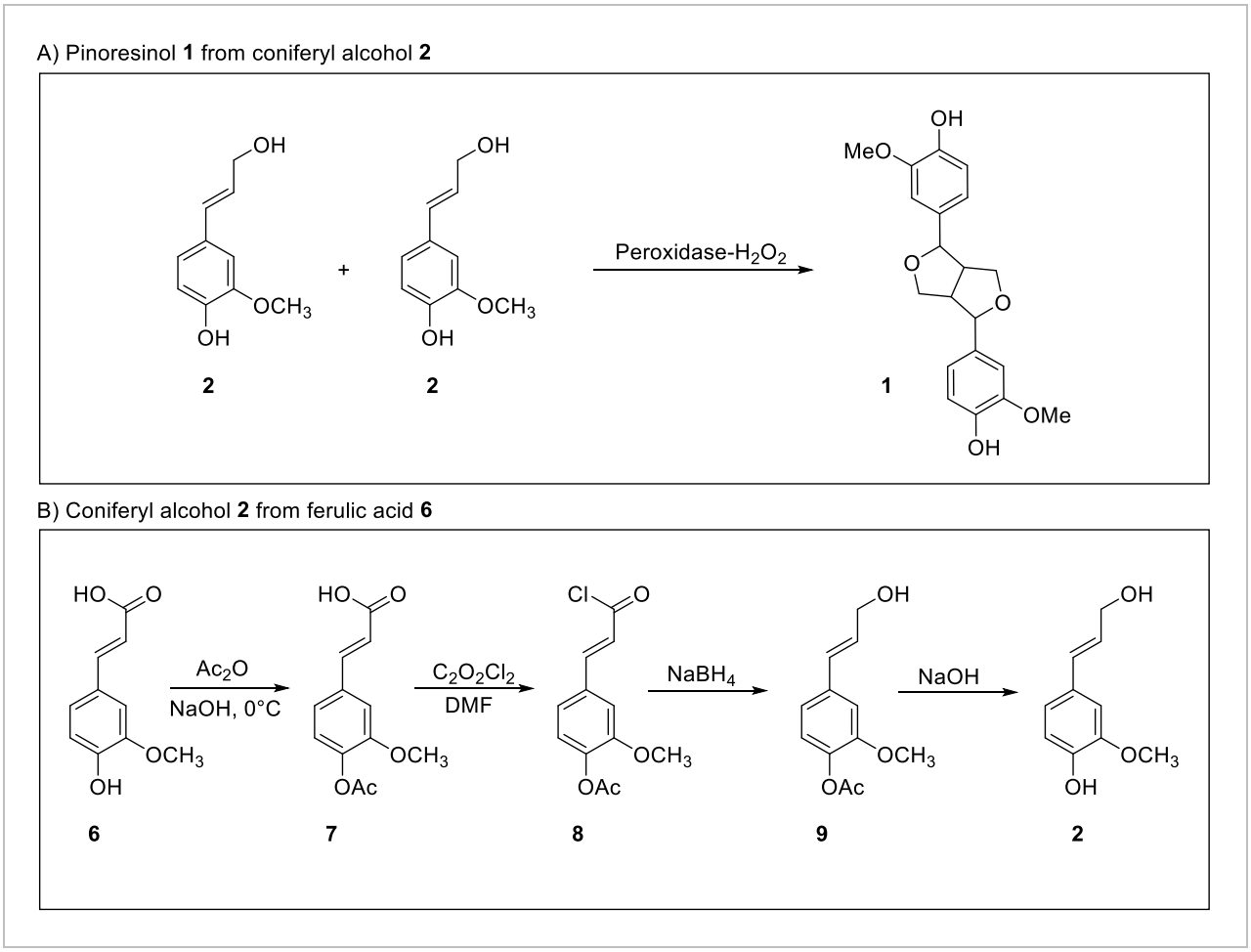

Figure 8. A) General principle of l Pinoresinol **1** synthesis form two Coniferyl alcohol **2** molecules according to Yue et al. (2021)[13]. B) Procedure of Coniferyl alcohol **2** synthesis from Ferulic acid **6** according to Panzella et al. (2018)[87] and Hosoda et al. (2001)[88].

3.2 Materials and Instrumentation

The purchased chemicals and materials used in this work are listed in Table 2. The table also shows the chemical purities and suppliers.

Table 2. Purchased chemicals and materials, their purities, and suppliers used in this work.

Compound	Purity	Supplier
Acetic acid	99.8%	Sigma-Aldrich
Acetic anhydride	≥99%	Sigma-Aldrich
Acetonitrile	99.9 %	VWR Chemicals
Dichloromethane	≥99.5%	Sigma-Aldrich
Dimethylformamide	99.5%	Fisher Scientific
Ethanol absolute	99.8%	VWR Chemicals
Ethyl acetate	99.5%	Fisher Scientific
Ferulic acid	99.0%	Sigma-Aldrich
Formic acid	99-100%	VWR Chemicals
Hydrochloric acid 1M	-	Fisher Chemical
Methanol	99.9%	Fisher Scientific
n-Hexane	97.0%	Thermo scientific
Orthophosphoric acid	85%	VWR Chemicals
Potassium hydroxide	99.98%	Fisher Scientific
Sand - low iron	-	Fisher Scientific
Silica gel 60	-	VWR Chemicals
Sodium dihydrogenphosphate 1-hydrate	99.0 %	Merck Millipore
Sodium hydroxide	≥97.0%	Sigma-Aldrich
tert-Butyl methyl ether	≥98%	Sigma-Aldrich

Ground *Picea abies* resin, and standards for BMB-A **3**, BMB-Al **5**, and BMB-OH **4**, were in-house sourced.

Liquid transfers in context with dilutions and standard preparation were conducted using volume-adjustable automated pipettes (Finnpipette F2, 20-200 µL; Finnpipette F2, 100-1000 µL) purchased from Thermo Scientific. All compounds were weighed with analytical balances (Mettler AE200). For solution requiring heating/stirring were prepared on a stirrer hot plate model RCT basic purchased from IKA-Werke. Reaction requiring controlled heating was conducted within a Hewlett 5890 Gas Chromatography oven located in a fume hood. Dissolution of initial reaction mixture for the homogeneous Cannizzaro protocols was supported by heating with a Park Side heat gun (Model PHLG 2000 E4). Büchi Rotavapor RII evaporator was used in the evaporation of extraction fractions.

Liquid chromatographic experiments were conducted using an Agilent Series 1260 HPLC instruments, consisting of a G1322A Degasser, a G1312B Binary Pumping System, G1329B Automated Liquid Sampler, a HP Series 1100 G1316A Thermostated Column Compartment, and an HP Series 1100 G1315A Diode Array Detector. The HPLC column used mobile phases, detected wavelengths, injection modes, and column temperatures used in all measurements can be seen in Table 3.

Table 3. HPLC column, mobile phases with acetonitrile (ACN) and formic acid (FA), detected wavelengths, injection mode, and column temperature used in the measurements.

Column	Luna 5 µm C18 (100 x 3.0 mm i.d.) @ Pre-column	
Mobile phases	**A** H2O-ACN-FA 95:5:0.05 (% v/v)	**B** H2O-ACN-FA 5:95:0.05 (% v/v)
Detection wavelength	210, 230, 254, 280, and 355 nm	
Injection Mode	Injection & Needle Wash, Wash Position: Vial11	
Column Temp.	25 °C	

Several different HPLC methods were used depending on the measurement needs. The properties of these methods and the method names used in this work can be seen in Table 4.

Table 4. HPLC method names and corresponding gradient profiles, injection properties, and flowrates.

Method name	Gradient profile	Injection volume (µL)	Flowrate (mL/min)
Grad_10B_35min	10% B for 0-10 min 10% B to 100% B in 10-30 min 10% B for 31-35 min	2	1
Iso-45B_10min	45 % B for 10 min	2	1

3.3 Experimental methods

3.3.1 Resin extraction and column chromatography of extracts

Pinoresinol **1** was extracted from in-house sourced, ground *Picea abies* resin using multi-solvent sequential hot extraction followed by mCC and CC for extract separation. The general workflow is depicted in Figure 9 A), and the extraction setup is illustrated in Figure 9 B). Table 5 lists the solvents used in the extraction, their respective volumes, and the extraction times. Solvents were selected based on polarity to optimize Pinoresinol **1** extraction while minimizing impurities.

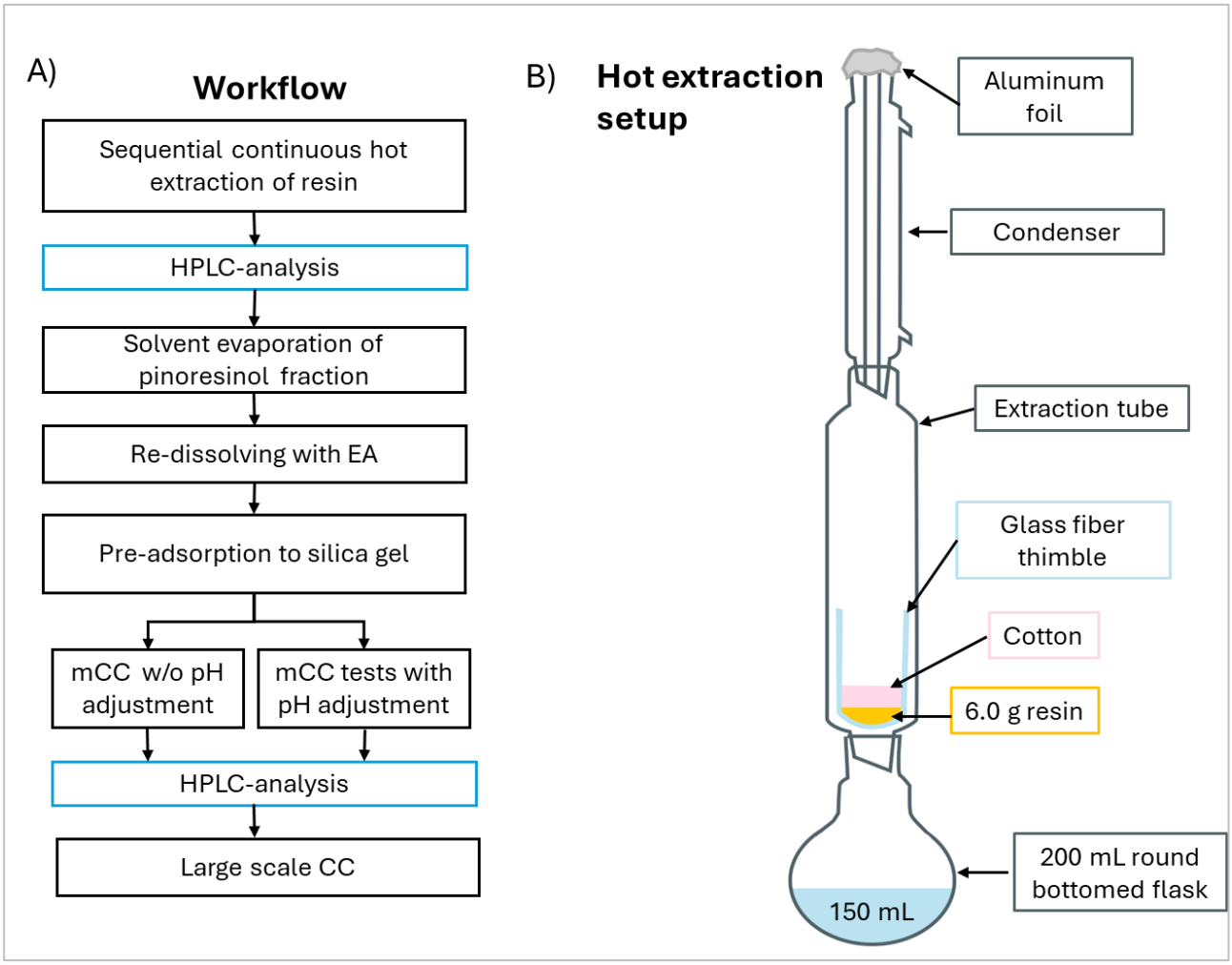

Figure 9. A) The workflow of Pinoresinol **1** extraction and separation with mCC and CC. B) An illustration of the multi-solvent sequential hot extraction setup used in this work.

First, 6.0 g of resin was weighed into a pre-weighed glass fiber thimble. A cotton plug was placed above the resin to prevent displacement during handling. The thimble was then inserted into a glass extraction tube, which was connected to a Liebig condenser. To minimize contamination, the top of the condenser was sealed with aluminum foil. A pre-weighed 200 mL round-bottom flask with a ground glass joint was attached below the extraction tube. To ensure accuracy and prevent cross-contamination, a new pre-weighed round-bottom flask was used for each solvent. A 2 cm magnetic stirrer was placed in the flask, and a heating mantle was used to bring each solvent to its respective boiling points. Extractions were performed systematically from lowest polarity towards higher.

Table 5. Solvents, extraction times, and names of extracts used in the multi-solvent sequential hot extraction of *Picea abies* resin. The extractions were performed from top to bottom order as listed in the table.

Extract name	Solvent	Solvent volume (mL)	Time (h)
HEX	n-Hexane	150	7
tBME	Tert-butyl methyl ether	150	7
EA	Ethyl acetate	150	7
MeOH1	MeOH	150	5
MeOH2	MeOH	150	5

After each extraction, the flasks were reweighed. A precipitate was observed in the n-Hexane extract, which was subsequently dissolved by adding 10 mL of EA to each sample.

HPLC samples were prepared from each extract to identify which extracts contained Pinoresinol **1**. For the samples, 500 µL of each extract was pipetted into HPLC vials using a 1 mL volume adjustable pipette. The solvents were then evaporated under nitrogen flow. After complete evaporation, 1 mL of ethanol was added by pipetting 500 µL twice with a 1 mL volume adjustable pipette. All vials were centrifuged at 4000 rpm for 4 minutes to prevent potential particulate contamination of the HPLC column. The HPLC method parameters are detailed in Table 4 (Grad_10B_35min). Based on the HPLC analysis results, the tBME fraction was dried using a rotary evaporator and then weighed.

The tBME extracts were pre-adsorbed in silica gel 60 for mCC and CC. First, the dried extract was redissolved in 60 mL of EA within the same flask. The solution was then mixed with 25 g of silica gel with the extract solution, followed by solvent evaporation using a rotary evaporator. The resulting pre-adsorbed silica exhibited a light yellowish color. Pre-adsorption was performed to mitigate solubility issues that may arise when loading extractables in liquid form.

A preliminary mCC was performed using 500 mg of the pre-adsorbed silica. An illustration of the column setup can be seen in Figure 10. The micro column was prepared using a 5 mL plastic pipette tip. A cotton plug was placed at the bottom of the pipette to prevent silica loss. Next, 1.53 g of silica 60 gel was mixed with n-Hexane in a headspace vial and added to the column. The column was equilibrated by passing approximately 15 mL of n-Hexane through it. Then, 500 mg of the pre-adsorbed silica was carefully added to the top of the column. To remove potential air bubbles, the pre-adsorbed layer was gently mixed using a Pasteur pipette. The final packed column length was approximately 10 cm, with a packing volume of approximately 4 mL. The column could accommodate an additional 8–9 mL of solvent above the packing. Following column packing, 12 fractions of 10 mL each were collected using a stepwise elution approach to evaluate whether increasing EA concentrations in MeOH would facilitate effective enrichment of Pinoresinol **1**. The protocol followed Table 6, except that AcOH was omitted. Following elution, a 1 mL HPLC sample was prepared from each fraction by pipetting 500 µL twice into an HPLC vial using a 1 mL adjustable pipette. For the MeOH fraction, only a 500 µL sample was taken due to its anticipated higher concentration of analytes. The solvent was subsequently evaporated from the samples using a nitrogen flow. The dried samples were then reconstituted by adding 500 µL of ethanol to each vial using the same pipette. To prevent particulate contamination of the HPLC instrument, all samples were centrifuged at 4000 rpm for 4 minutes. A gradient HPLC analysis was performed for the samples using Grad_10B_35min method (Table 4). Analysis of the eluents revealed that Pinoresinol **1** eluted broadly across multiple fractions with significant amounts of impurities, indicating insufficient separation.

To improve this, a second mCC experiment was conducted using 4.9 g of pre-adsorbed silica, maintaining the same column setup and fractionation scheme as outlined in Table 6. In this experiment, AcOH was added to adjust the pH, ensuring that acidic components remained in their protonated form. This modification aimed to achieve more concentrated Pinoresinol **1** elution with reduced impurities. HPLC samples were prepared and analyzed as described previously.

Table 6. Fraction names and compositions determined for Pinoresinol **1** separation from tBME extract for mCC. The procedure was performed systematically from top row to bottom.

Fraction name	V(EA) (mL)	V(MeOH) (mL)	V(AcOH) (µL)	V(fraction) (mL)
EA10	1	9	100	10.1
EA20	2	8	100	10.1
EA30	3	7	100	10.1
EA40	4	6	100	10.1
EA50	5	5	100	10.1
EA60	6	4	100	10.1
EA70	7	3	100	10.1
EA80	8	2	100	10.1
EA90	9	1	100	10.1
EA100 1	10	0	100	10.1
EA100 2	10	0	100	10.1
MeOH	0	10	100	10.1

The mCC method (Table 6) with AcOH was adapted to conventional column chromatography in 30-fold solvent volumes and 10-fold sample amounts (Figure 10). The glass column had a diameter of approximately 5.5 cm and was packed with 45.6 g of silica gel 60, forming a 5.5 cm tall layer. Subsequently, 15.0 g of the previously prepared pre-adsorbed silica gel was added to a layer of 0.5 cm above the pure silica gel 60. The extractable mass was approximately 2.2 g in the 15 g of pre-adsorbed silica gel. To prevent disturbance of the pre-adsorbed silica gel during solvent addition, a 0.5 cm layer of low-iron fine sand was placed as a top layer. For HPLC analysis, a 1 mL sample was taken from each fraction as described previously.

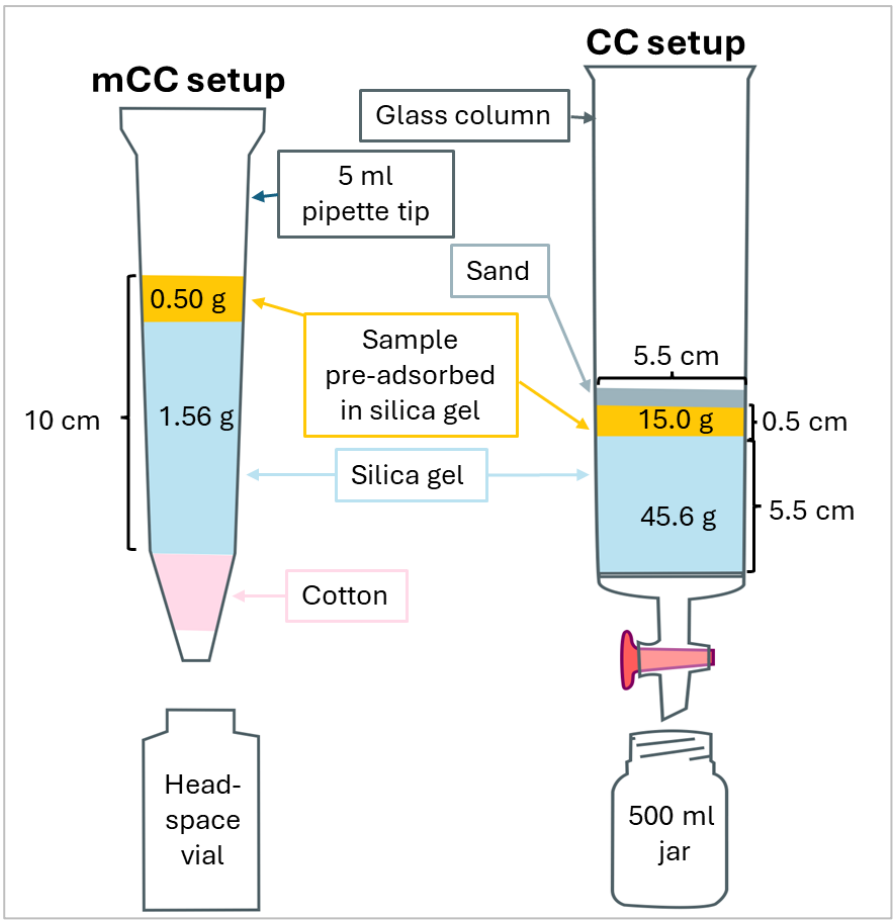

Figure 10. An illustration of the mCC and CC setup. The illustration is not to scale, and relevant dimensions have been marked in the figure.

3.3.2 Cannizzaro reaction

3.3.2.1 Homogeneous and heterogeneous reaction conditions

Two batches of Cannizzaro reactions of BMB-Al **5,** were performed. The reaction conditions were identical except for MeOH and KOH amount, which resulted in homogeneous and heterogeneous conditions. The workflows for homogeneous and heterogeneous Cannizzaro reactions can be seen in Figure 11.

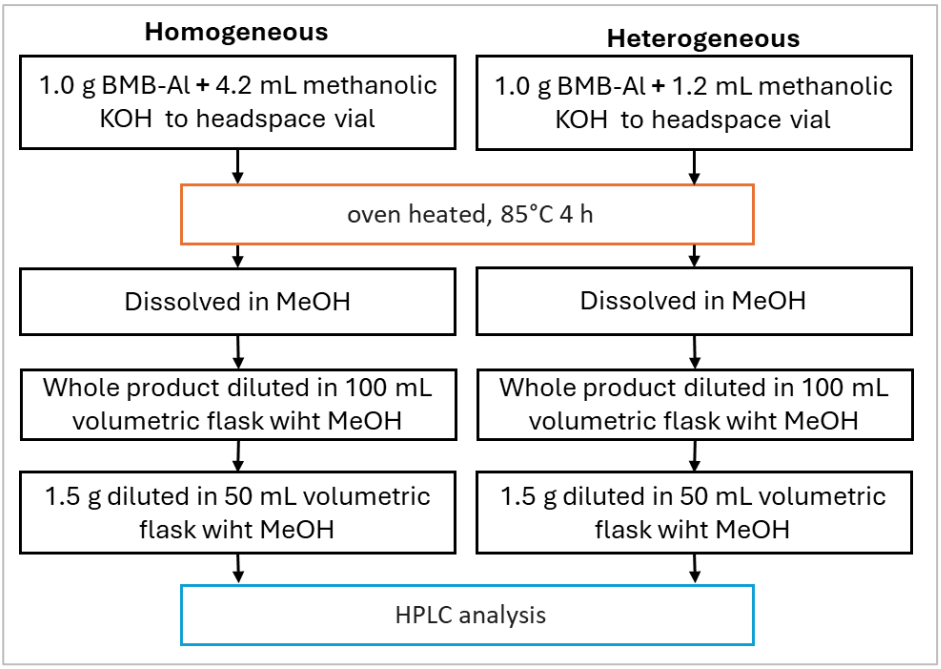

Figure 11. Schematic presentation of workflows for homogeneous and heterogeneous reaction conditions for Cannizzaro reaction of BMB-Al **5**.

Homogeneous Cannizzaro reaction of BMB-Al **5** was adapted from Singh et al. (2007)[16]. First, 100 mL Erlenmeyer flask with a ground glass joint was charged with 3.33 g (59.4 mmol) KOH, followed by 20 mL of MeOH and a 3 cm magnetic stir bar. The mixture was mounted on a stirrer hot plate and loosely sealed with a polypropylene stopper and gently agitated until complete dissolution of the KOH. Subsequently, 1.01 g (4.17 mmol) BMB-Al **5** was weighed into a 20 mL headspace vial, and 4.20 mL of the prepared methanolic KOH solution containing approximately 0.83 g (14.8 mmol) KOH was added by means of a 5 mL volume adjustable pipette. The vial was sealed with a septum cap and the white suspension heated with a heat gun with gentle shaking until all solids had been dissolved. The vial was then placed into a gas chromatography oven and heated at 85°C for 4 h. Visual inspection of the reaction vial after 0.5 h showed a slightly yellowish solution of oily looking consistence, which remained homogeneous over the entire reaction period. Subsequently, the vial was removed from the oven and allowed to cool to ambient temperature, upon which the contents solidified to a moist crystals mass.

For the heterogeneous conditions, A 100 mL Erlenmeyer flask with a ground glass joint was charged with 5.0 g (89.1 mmol) solid KOH, followed by 8 mL of methanol and a 3 cm magnetic stir bar. The mixture was mounted on a hot stirrer plate and loosely sealed with a polypropylene stopper, and then gently agitated until the majority of the added KOH had dissolved. A minority of solid KOH was observed to remain undissolved. Subsequently, 1.01 g (4.15 mmol) BMB-Al **5** was weighed into a 20mL headspace vial. Then, 1.20 mL of the prepared methanolic KOH solution, containing approximately 0.50 g KOH, corresponding to 8.9 mmol, was added in portions using 1 mL and 500 µL volume-adjustable pipettes. Only a minor portion of the BMB-Al **5** was observed to dissolve upon the addition of the KOH solution, and a thick colorless suspension was obtained. The vial was sealed with a septum cap and then placed into a gas chromatography oven and heated at 85°C for 4 h. Visual inspection of the vial after 0.5 h showed that the suspension had turned into a solid mass of colorless crystals, which remained essentially unchanged over the entire reaction period. Subsequently, the vial was removed from the oven and allowed to cool to ambient temperature.

The Cannizzaro products were dissolved in MeOH for analysis. First, 5 mL of MeOH was added to the headspace vials containing the homogeneous and heterogeneous Cannizzaro reaction mixtures respectively. The mixture was manually shaken until the solid had been completely dissolved. The solutions were transferred with glass funnels into their own 100 mL volumetric flasks. The headspace vials were rinsed with fresh MeOH (3 × 5 mL), and the washings were combined with the corresponding solutions in the volumetric flasks. The flasks were then filled to mark with MeOH. A dilution was performed from the 100 mL whole product dilution. First, 1.53 g of the homogeneous reaction solution and 1.54 g of the heterogeneous solution were pipetted to their own 50 mL volumetric flasks. The flasks were then filled to the mark with MeOH and homogenized by shaking. Out of both mixtures three samples were taken for HPLC analysis. The samples were taken by pipetting approximately 500 µL to HPLC vials using a glass Pasteur pipette. The HPLC vials were closed with a stopper and analyzed using an isocratic HPLC method (Iso-45B_10min, Table 4). Two MeOH blank samples were run between each sample to avoid analyte bleeding between samples.

3.3.2.2 Calibration series sample preparation

For calibration, common stock solutions were prepared for BMB-Al **5**, BMB-A **3**, and BMB-OH **4** using in-house standards. The standards used were synthesized in-house prior to this experimental work. The common stock solutions were prepared by weighing 1.46 g (6.0 mmol) of the BMB-Al **5**, 1.02 g (3.9 mmol) of BMB-A **3**, and 1.05 g (4.3 mmol) of BMB-OH **4** into their respective 100 mL volumetric flasks. Approximately 50 mL of ACN was added to each flask, and the solids were dissolved and homogenized with manual shaking. Then, the flasks were filled to the mark with ACN. A diluted multi-component mixed standard stock solution was prepared from the stock solutions to a pre-weighed 50 mL volumetric flask as. First, 3 mL aliquots of each common stock solution were pipetted to the 50 mL flask as seen in Figure 12. The aliquots were pipetted in 1.5 mL increments using a 5 mL volume-adjustable pipette and the flask was re-weighed after each addition with the stopper on. The flask was then filled to the mark with ACN, re-weighed, sealed with a polypropylene stopper, homogenized by shaking.

The calibration series were prepared in HPLC vials through diluting the mixed standard with ACN. The dilution protocol can be seen in Table 7 and in Figure 12.

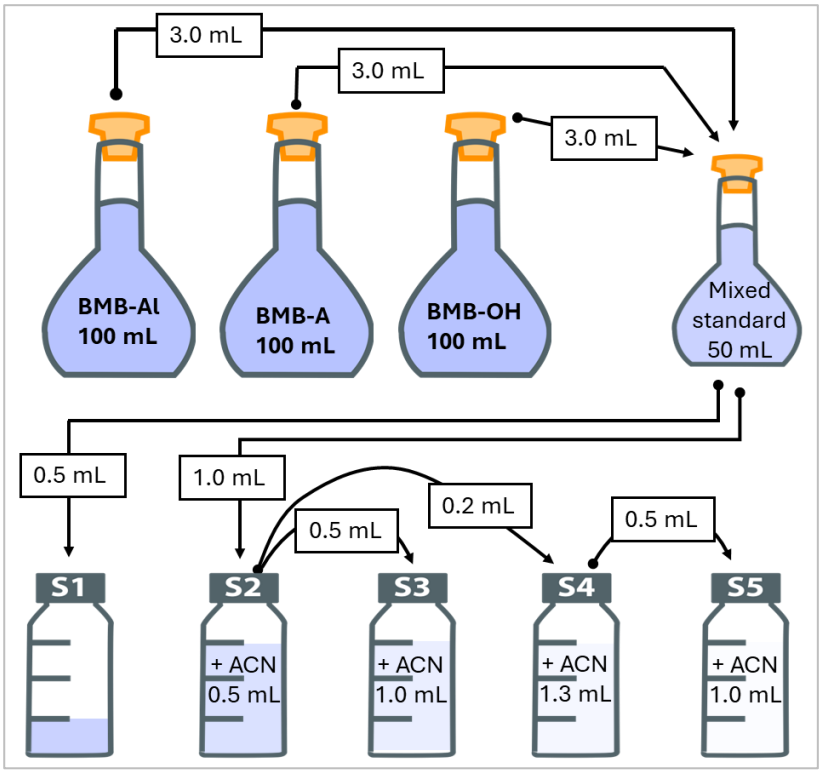

Figure 12. Schematic presentation of the preparation of the mixed standard and the dilutions for the calibration standards s1-s5. The addition of ACN to the mixed standard has been left out of to improve readability.

All dilutions were done using volume adjusting pipettes (1000, 500 and 100 µL). The pipetting was done in sections in a manner where at most 50% of the pipettes volume was pipetted at a time. The empty vials were pre-weighed and re-weighed after the addition of standard and solvent respectively. All weighing's were done with the cap secured. Since the pipetted volumes were small, special attention was paid to keeping the HPLC vials open as little as possible and adding ACN as fast as possible to the weighed standard to avoid evaporation of solvent. After each standard was done, the closed vials were gently shaken for homogenization. The mixed standard was used as the highest concentration of the calibration series (s1). Standards 2 and 3 (s2 and s3), were diluted from the stock mixed standard. Standards 3 and 4 (s3 and s4) were prepared from s2 and standard 5 (s5) was prepared from homogenized s4 as seen in Table 7.

Three sets of standard series were prepared for one calibration repetition, and six separate calibration repetitions were done in total as described before. The series were then analyzed using an isocratic HPLC method (Iso-45B_10min, Table 4). To blank ACN samples were run between each standard series and the standards were analyzed in order from most diluted towards more concentrated.

Table 7. Dilution protocol for the calibration series.

Standard	Standard diluted	V(Standard diluted) (mL)	V(ACN) (mL)	V(Final) (mL)
s1	Mixed standard	0.5	0	0.5
s2	Mixed standard	1.0	0.5	1.5
s3	s2	0.5	1.0	1.5
s4	s2	0.2	1.3	1.5
s5	s4	0.2	1.3	1.5

3.3.3 Pinoresinol **1** precursors from ferulic acid **6**

*3.3.3.1 4-Acetoxyferulic acid **7***

4-Acetoxyferulic acid **7** was prepared by acetylation of Ferulic acid **6** with acetic anhydride in alkaline aqueous solution. First, a 250 mL Erlenmeyer flask with a ground glass joint was charged with 2.62 g (56.5 mmol) NaOH and a 2 cm magnetic stir bar. The flask was fitted with a 2-necked Claisen adapter, with one neck carrying an inert Teflon gas line and the other a septum for reagent addition. After immersion of the flask into an ice-water bath, 40 mL water was added and the mixture stirred until complete dissolution of the solids. The flask was purged with a stream of nitrogen for 5 min to replace air. Then, 7.79 g (40.0 mmol) of Ferulic acid **6** was added in a single portion, which quickly dissolved to form a bright yellow solution. The measurement of pH of the mixture using test paper indicated pH > 10. Then, 6.50 mL (7.02 g, 62.0 mmol) of acetic anhydride was added via the Teflon capillary dropwise to the stirred mixture over a period of 25 min.

The color of the reaction mixture gradually faded during addition. After the addition, the mixture was stirred for 25 min period at 0°C, during which a small amount of a slightly yellowish solid started precipitating. At this point, the pH of the mixture had dropped to 6-7. The heterogeneous mixture was removed from the ice-water bath and transferred to a 500 mL beaker together with a 5 cm magnetic stir bar. The mixture was diluted with sufficient water to bring the total volume of 300 mL. Then, the pH of the mixture was adjusted to pH 3–4 by the addition of 130 mL of 1 M HCl, resulting in a voluminous white suspension. After stirring for another 20 min at an ambient temperature, the precipitate was isolated by filtration through a pre-weighed Buchner funnel. The filtrate was then washed repeatedly with de-ionized water (3 x 50 mL). The funnel containing the solid was covered with aluminum foil and placed into a ventilated gas chromatography oven and dried at 60°C for 24 h. A HPLC sample was taken by dissolving a few crystals of the crude product in approximately 0.5 mL of ACN in a HPLC vial.

For purification, the crude product was recrystallized from absolute ethanol. For this purpose, the crude material was loaded into an extraction thimble, which was then loosely covered with a cotton plug. The loaded thimble was inserted into a continuous hot extraction apparatus, consisting of a heating mantle holding a 500 mL round-bottomed flask and a 3 cm egg-shaped stir bar, a column-shaped extraction compartment, and a reflux condenser. Absolute ethanol (170 mL) was carefully applied via a long-stemmed glass funnel onto the top of loaded thimble, permeating through and thus pre-wetting the sample. Then, the ethanol collected in the extraction flask was heated to boiling, with the hot vapors and refluxing liquid causing the gradual dissolution of the crude product. After 4 h, the crude product initially present in the thimble had been completely dissolved, generating a clear yellowish solution in the extraction flask. At this point, heating was switched off and the extraction solution was allowed to cool slowly to ambient temperature, upon which crystallization occurred. For the completion of the crystallization, the extraction flask was sealed with a polypropylene stopper and transferred to a -20°C freezer. After 24 h, the crystal mass was collected in a pre-weighed filter funnel. Of the mother liquor, an approximately 0.2 mL sample was taken to a HPLC vial with a glass Pasteur pipette. The sample was then evaporated to dryness under nitrogen flow and re-dissolved in ACN for HPLC analysis. The purified product was washed repeatedly with ice-cold absolute ethanol (2 x 10 mL). The filter funnel containing the recrystallized product was dried in a ventilated gas chromatography oven for 24 h. A HPLC sample was taken of the purified product by dissolving taken by dissolving a few crystals of the crude product in approximately 0.5 mL of ACN in a HPLC vial. The HPLC samples from crude and purified products, and the mother liquor were analyzed using a gradient HPLC analysis (Grad_10B_35min, Table 4).

Two additional synthesis runs carried out under identical conditions using 3.88 g (19.9 mmol) of Ferulic acid **6**.

*3.3.3.2 4-Acetylferuloyl chloride **7***

4-Acetylferuloyl chloride **8** was prepared from the previously prepared 4-Acetoxyferulic acid **7**. For the reaction, 1.09 g (4.7 mmol) of 4-acetoxyferulic acid **7** was added to a 200 mL round-bottom flask. Approximately 40 mL of dichloromethane was then added, and the resulting heterogeneous mixture was stirred using a 4 cm magnetic stir bar. The reaction was conducted under light-protected conditions while stirring. Subsequently, 20 µL of catalyst dimethylformamide and 600 µL (0.89 g, 7.0 mmol) of oxalyl chloride were added to the mixture. At the start, the reaction mixture was colorless and heterogeneous. After 25 minutes at room temperature, the solution became homogeneous with a slight yellow tint. Stirring continued for an additional 70 min. Following the reaction, the solvent was removed via rotary evaporation, yielding a slightly yellow solid product.

*3.3.3.3 4-Acetoxyconiferyl alcohol **9***

4-Acetoxyconiferyl alcohol **9** was prepared by reducing the previously synthesized 4-Acetylferuloyl chloride **8**. For the synthesis, $NaBH_4$ was dried in a gas chromatography oven at 150°C for several days. Then, 0.99 g (3.9 mmol) of 4-Acetylferuloyl chloride **8** was weighed into a 200 mL round-bottom flask equipped with a ground glass joint. Subsequently, 60 mL of freshly distilled EA was added, dissolving the compound to form a clear slightly yellowish solution. The solution was then moved to a dropping funnel. Separately, 0.17 g (4.6 mmol) of $NaBH_4$ was dissolved in 70 mL of fresh EA. The dissolution was aided with a 2 cm magnetic stirrer. The flask and dropping funnel were then connected, and a bubbler was attached on top of the dropping funnel. An ice bath was applied to the $NaBH_4$ solution. The 4-Acetylferuloyl chloride **8** solution was then added dropwise via capillary over 35 minutes. The reaction mixture gradually turned milky white over this time and gas formation was observed during the reaction. To monitor the reaction progress, HPLC samples were taken at 10 minutes, 2 hours, 6 hours 45 minutes, and 1 day 3 hours of stirring. Samples were prepared by evaporating approximately 200 µL of the reaction mixture under a nitrogen gas flow, followed by re-dissolution in 1 mL of EtOH. Notably, bubbling was observed upon EtOH addition, indicating the presence of active reagents still in the mixture. Based on the results of the analysis, the synthesis series was not continued.

3.4 Results of experimental work

3.4.1 Resin Extraction and Column Chromatography

According to the literature, approximately 12 m-% of *Picea abies* resin consists of Pinoresinol **1**.[82] Based on this value, approximately 0.7 g of Pinoresinol **1** was present in the 6.0 g of resin extracted in this work. The HPLC analysis of the extracts showed that the majority of Pinoresinol **1** was extracted into the tBME fraction (Figure 13.) It can be seen from the chromatogram that many major impurities extracted with Pinoresinol **1** in the crude extract. The dry extractable mass of the tBME fraction was 3.60 g

Chromatograms of the other extracts can be seen in Appendix 1. MeOH2 fraction is excluded from the overlay due to the chromatogram lacking distinguishable peaks.

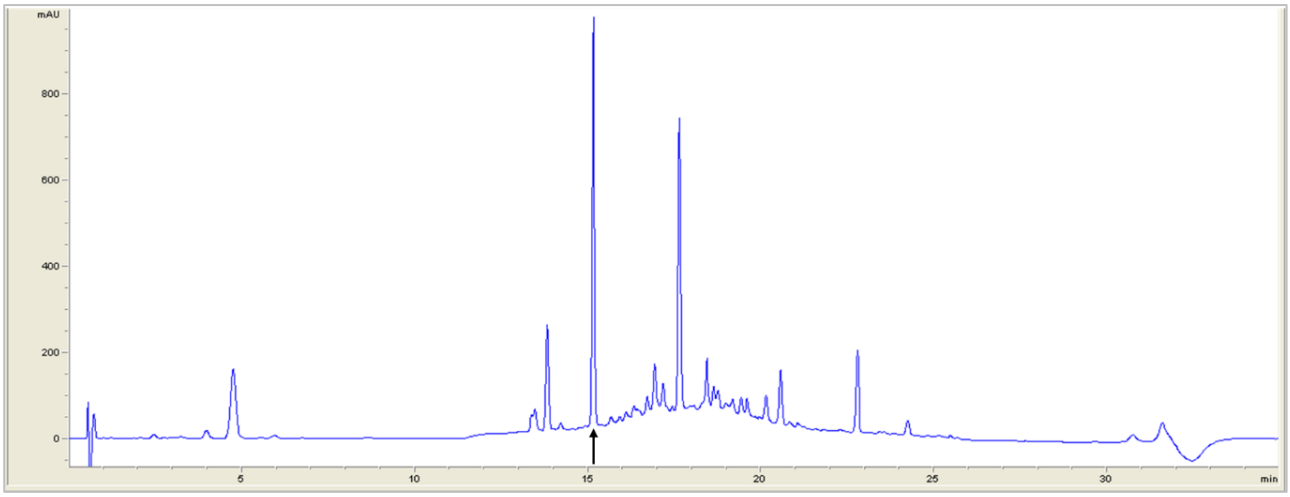

Figure 13. Chromatogram from tBME extract. Pinoresinol **1** is marked in the figure with a black arrow.

The analysis of the CC results showed that Pinoresinol **1** eluted narrowly in the EA50 fraction. Some tailing of Pinoresinol **1** was observed in the EA 60 fraction also. The fractions EA40, EA50 and EA60 can be seen overlaid with the tBME fraction in Figure 14. One notable impurity peak can also be seen in the EA50 fraction. Approximately 2.2 g of the tBME extractables were loaded to the CC through the pre-adsorbed silica. This corresponds to approximately 0.4 g of Pinoresinol **1,** if it is approximated that the total 0.7 g of Pinoresinol **1** was extracted to the tBME fraction.

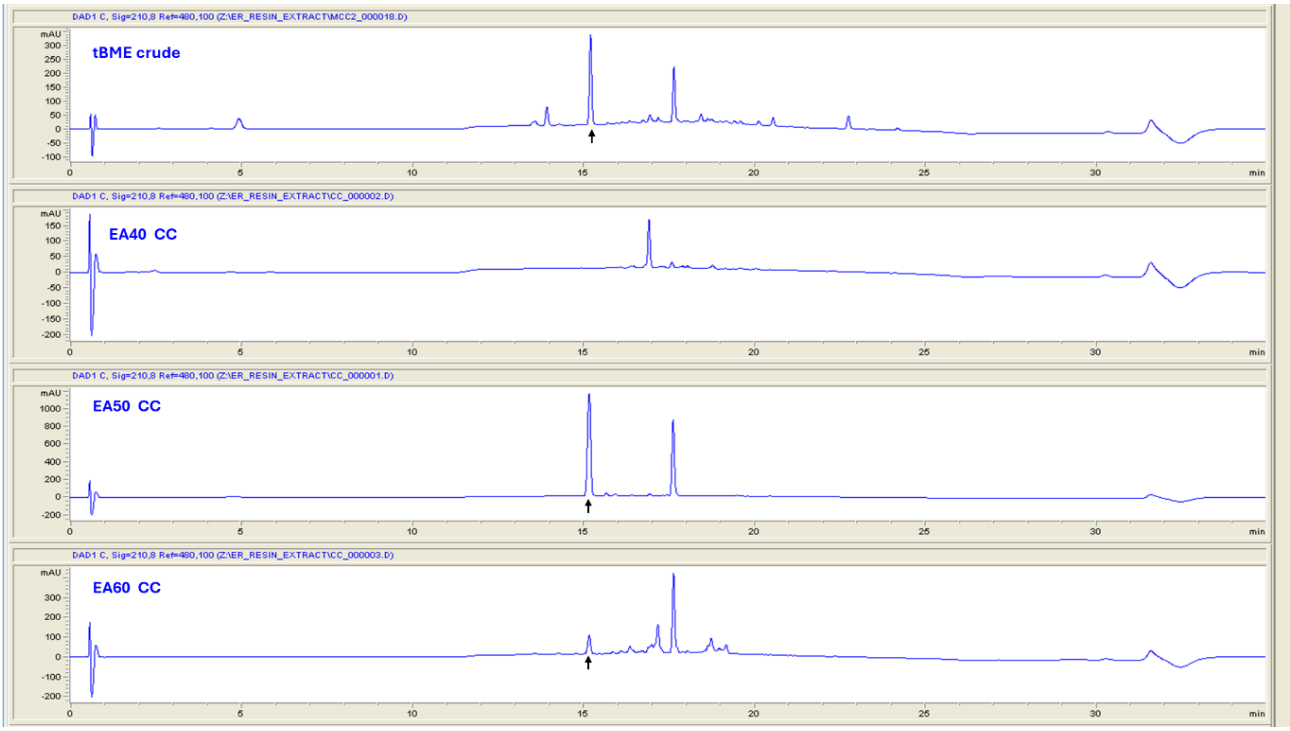

Figure 14. tBME crude, and fractions EA40, EA50 and EA 60 from CC. Pinoresinol **1** is marked in the chromatograms with a black arrow.

3.4.2 Calibration method for Cannizzaro reaction analysis

The signal to noise ratio (S/N) was determined from the peak height of the lowest calibration standards and the noise level at the site of the peak's taken from a blank ACN sample. The comparison of all measured wavelengths regarding S/N for all three Cannizzaro compounds can be seen in Appendix 2. The results showed that 280 nm had superior S/N compared to the other measured wavelengths. However, BMB-A **3** did not absorb this wavelength as strongly as the other two compounds. Consequently, the 230 nm wavelength was selected for calibration, as it provided the most consistent S/N ratio across all measured compounds. Based on these S/N values, the LOD and LOQ were calculated for the Cannizzaro compounds. The LOD and LOQ values are presented in Table 8 and in Appendix 3.

The calibration series were plotted as the injected mass of standard against the average peak area of the three measured series for BMB-Al **5**, BMB-A **3**, and BMB-OH **4**, respectively. An example full set of chromatograms for one measured calibration series can be found in Appendix 4. Linear fits were applied to the data with the least squares method to get calibration equations. From the slopes of the resulting equations, the relative standard deviation (RSD) values were calculated for each compound. The slopes, their averages, and

values from all six repetitions are presented in Table 8. The results show that the RSD values are approximately 1% or lower for all compounds, demonstrating satisfactory repeatability. The intercepts of the regression fits were excluded from consideration, as they were below 1% of the slope and could be attributed to experimental error.

Table 8. Slopes of calibration series obtained through regression analysis, the average of the slopes and the slope RSDs for the Cannizzaro compounds.

	BMB-Al	BMB-A	BMB-OH
Slope 1	3375.5	2362.8	2091.8
Slope 2	3297.3	2312.2	2120.9
slope 3	3365.0	2377.8	2086.0
slope 4	3380.5	2359.7	2095.7
slope 5	3323.7	2374.0	2069.8
slope 6	3336.0	2389.0	2093.0
Average slope	3346.3	2362.6	2092.9
Slope RSD	0.90	1.04	0.72

3.4.3 Yields and product purities of the Cannizzaro reactions

The theoretical yields of BMB-A **3** and BMB-OH **4** were determined based on the substance amount of BMB-Al **5**. The theoretical yields of the heterogeneous reaction conditions were calculated to be 538.0 mg for BMB-A **3** and 508.9 mg for BMB-OH **4**. For homogeneous conditions the theoretical yields were calculated to be 535.7 mg for BMB-A **3** and 506.7 mg for BMB-OH **4**.

The concentrations of the BMB-Al **5**, BMB-A **3**, and BMB-OH **4** were first calculated in the 50 mL MeOH dilutions based on the average peak areas measured and the average calibration slopes (Table 8). Overlaid chromatograms (230 nm) of the Cannizzaro reaction products in both studied conditions can be seen in Appendix 5. The total yields in the 100 mL volumetric flasks were then calculated based on the mass diluted to the 50 mL flasks and the density of MeOH. The calculated yields, average peak areas and % of the yield of the theoretical yields can be seen in Table 9. It can be seen from the results, that the homogeneous reaction conditions produced significantly more of both BMB-A **3**, and BMB-OH **4** and had less starting material left over. The small BMB-Al **5** peak in the heterogeneous conditions was above the LOQ peak height (Appendix 2).

Table 9. Average peak areas, and calculated masses for starting material BMB-Al **5** and products BMB-A **3** and BMB-OH **4**. The % of theoretical yields of the products are also shown in the table.

Heterogeneous conditions

Compound	Average peak area	Total mass (mg)	% of theoretical yield
BMB-Al	18.9	7.2	-
BMB-A	955.8	517.6	96.2
BMB-OH	780.4	481.7	94.7

Homogeneous conditions

Compound	Average peak area	Total mass (mg)	% of theoretical yield
BMB-Al	566.7	218.5	-
BMB-A	602.4	326.2	60.6
BMB-OH	533.7	329.5	64.7

The amounts of substance of the products and leftover starting material were compared to the amount of substance of the starting material for both studied conditions. Based on the comparison, 0.6 mmol of side products formed in homogeneous conditions. This corresponds to 15.2% of the BMB-Al **5** starting material substance amount. In the heterogeneous conditions 0.2 mmol of side products were formed, which is 3.9% of the BMB-Al **5** starting material substance amount.

3.4.4 4-Acetoxyferulic acid **7,** 4-Acetylferuloyl chloride **8**, and 4-Acetoxylconiferyl alcohol **9**

The crude yield of 4-Acetoxyferulic acid **7** was 8.97 g, (95% of theoretical yield) and the recrystallized yield was 8.10 g (0.035 mmol, 88% of theoretical yield) of white crystals. HPLC analysis (210 nm) indicated a product purity of 96% and the presence of 4% of residual Ferulic acid **6**. The overlaid chromatograms of crude and recrystallized products, along with the mother liquor from recrystallization, are provided in Appendix 6. The two repetitions of the 4-Acetoxyferulic acid **7** each gave similarly favorable results. Subsequent synthesis of 4-Acetylferuloyl chloride **8** resulted in a yield of 0.989 g, corresponding to 128% of the theoretical yield. A yield exceeding 100% suggests the presence of impurities, insufficient drying of the product, or both. The HPLC analysis (210 nm, Appendix 6) results of the reduction of 4-Acetylferuloyl chloride **12** to 4-Acetoxylconiferyl alcohol **9** indicated an incomplete reaction after 1 day and 3 hours (Appendix 7). HPLC samples taken at 10 minutes, 2 hours, and 6 hours 45 minutes showed progressive reduction of 4-Acetylferuloyl chloride **8**. However, no further progression was observed beyond this point. The chromatogram at 1 day and 3 hours shows partial reversion of **4-**Acetoxylconiferyl alcohol **9**

back to 4-Acetylferuloyl chloride **8**. Due to this observed regression, the synthesis sequence to produce Coniferyl alcohol **2** was discontinued.

3.5 Conclusions and discussion of experimental work

In this study, Pinoresinol **1** was successfully extracted from 6.0 g of *Picea abies* resin using multi-solvent sequential hot extraction. Based on literature data,[82] it was estimated that 0.7 g of Pinoresinol **1** could be separated from the resin. HPLC analysis revealed that Pinoresinol **1** was primarily concentrated in the tBME extract, which yielded a total of 3.60 g of extractable material. For enrichment, approximately 2.2 g of extractables pre-adsorbed in silica gel were processed using CC. The CC method included 12 fractions, each with a volume of 300 mL, eluted with a gradient of increasing ethyl acetate concentration in methanol. The eluent pH was adjusted using acetic acid, which facilitated the concentration of the majority of Pinoresinol **1** into a single fraction. HPLC analysis demonstrated that a major impurity remained co-eluted with Pinoresinol **1**, although the purity was considerably improved compared to the crude tBME extract. The enrichment process required a total solvent volume exceeding 3.6 L. We estimated that the yield of purified Pinoresinol **1** was less than 0.5 g. Despite achieving enhanced purity, the persistence of a co-eluting impurity, combined with the substantial solvent consumption, indicates that this method is not suitable for Pinoresinol **1** standard production from an environmental and financial standpoint. Future research should focus on exploring more efficient and economically feasible strategies for Pinoresinol **1** enrichment.

A calibration method was developed for the quantification of the BMB-A **3**, BMB-Al **5**, and BMB-OH **4** to evaluate the success of the Cannizzaro reactions studied. The calibration was done with a mixed standard of all three compounds as a series of dilutions in HPL vials. The S/N analysis determined that 230 nm provided the most consistent sensitivity across all Cannizzaro compounds, making it the optimal wavelength for calibration. Six independent calibrations were done, and the slopes of the regression analysis were compared to assess repeatability. The RSD values of the slopes were ≤1%, indicating high repeatability. The LOQ limits are suitable for all analytes in both conditions, making the method suitable for the evaluation of the Cannizzaro synthesis.

The investigation into Cannizzaro protocols revealed that heterogeneous literature reaction conditions produced significantly higher yields compared to the theoretical yield. The yields of BMB-A **3** and BMB-OH **4** were 96.2% and 94.6%, respectively. In homogeneous conditions, the yield of BMB-A **3** was 60.6% and the yield of BMB-OH **4** was 64.7%. The

heterogeneous reaction conditions were more favorable in terms of formed side products. Under heterogeneous conditions, only 3.9% of the starting material was transformed into side products, whereas under homogeneous conditions, side product production accounted for 12.3% of the starting material. Based on the yields and side product formation, the heterogeneous reaction conditions are more favorable compared to the homogeneous conditions proposed in this work. We hypothesize that the superiority of the heterogeneous conditions can be readily rationalized considering the protective effects due to product precipitation. The precipitation of the products limits their exposure to the strongly basic medium and thus prevents any further base-promoted decomposition. Under homogeneous conditions, this protective effect is essentially absent. In this case, both BMB-A **3** and the BMB-OH **4** remain in the solution. Consequently, they are available to a broad range of base-promoted side reactions, such as oxidation, decarboxylation, and esterification. Moreover, the use of larger volumes of solvent under homogeneous conditions dilutes all reaction partners and slows the overall rate of the productive Cannizzaro reaction, which is evident from the considerable amount of unreacted aldehyde present under homogeneous conditions. Questions remain on whether heterogeneous conditions are suitable for scaling up the synthesis volume, as the solid phase observed in the reaction does not allow for stirring and could lead to uneven heating of the mixture in a larger scale experiment. However, for small-scale preparations this protocol, due to its cleanness and high yields, and use of inexpensive and green reagents, may offer significant advantages over alternative protocols.

The synthesis pathway tested for the production of Coniferyl alcohol **2** offered mixed results. The first step of 4-Acetoxyferulic acid **7** synthesis resulted in 88% yield with 96% purity. The following chlorination step did lead to a successful 4-Fcetylferuloyl chloride **8** production. However, the yield indicated that the product had either many impurities or solvent present, due to an above 100% yield. The final performed synthesis was the reduction of 4-Acetylferuloyl chloride **8** which resulted in an incomplete reaction with the product 4-Acetoxylconiferyl alcohol **9** degrading back to 4-acetylferuloyl chloride as the reaction proceeded. Due to the degrading product, this reaction pathway was concluded to be unsuitable for Coniferyl alcohol **2** synthesis. Based on this experimental work it would be beneficial to find other alternatives for Coniferyl alcohol **2** synthesis.

References

1 G. M. Cragg and D. J. Newman, *Biochim. Biophys. Acta BBA - Gen. Subj.*, 2013, **1830**, 3670–3695.
2 A. G. Atanasov, B. Waltenberger, E.-M. Pferschy-Wenzig, T. Linder, C. Wawrosch, P. Uhrin, V. Temml, L. Wang, S. Schwaiger, E. H. Heiss, J. M. Rollinger, D. Schuster, J. M. Breuss, V. Bochkov, M. D. Mihovilovic, B. Kopp, R. Bauer, V. M. Dirsch and H. Stuppner, *Biotechnol. Adv.*, 2015, **33**, 1582–1614.
3 J. Jokinen and A. Sipponen, *Adv. Wound Care*, 2014, **5**, 140120074901006.
4 J. Zuo, P. Ma, Z. Li, Y. Zhang, D. Xiao, H. Wu and A. Dong, *Macromol. Mater. Eng.*, 2023, **308**, 2200499.
5 F. M. Antony, D. Pal and K. Wasewar, *Phys. Sci. Rev.*
6 T. Jiang, R. Ghosh and C. Charcosset, *Trends Food Sci. Technol.*, 2021, **112**, 419–430.
7 L. Dinan, J. Harmatha and R. Lafont, *Gas Liq. Chromatogr. Non-Sapon. Lipids Part I*, 2001, **935**, 105–123.
8 J. B. Tse Sum Bui, A. Mier and K. Haupt, *Small*, 2023, **19**, 2206453.
9 M. Naseri, M. Mohammadniaei, Y. Sun and J. Ashley, *Chemosensors*.
10 Y. Li, L. Luo, Y. Kong, Y. Li, Q. Wang, M. Wang, Y. Li, A. Davenport and B. Li, *Biosens. Bioelectron.*, 2024, **249**, 116018.
11 C. Huang, H. Wang, S. Ma, C. Bo, J. Ou and B. Gong, *J. Chromatogr. A*, 2021, **1657**, 462579.
12 L. Markulin, C. Corbin, S. Renouard, S. Drouet, L. Gutierrez, I. Mateljak, D. Auguin, C. Hano, E. Fuss and E. Lainé, *Planta*, 2019, **249**, 1695–1714.
13 F. Yue, W. Lan, L. Zhang, F. Lu, R. Sun and J. Ralph, *Front. Energy Res.2021,* **9**
14 L. B. Davin, D. L. Bedgar, T. Katayama and N. G. Lewis, *Int. J. Plant Biochem.*, 1992, **31**, 3869–3874.
15 J. Maruyama, M. Kobayashi, M. Miyashita, I. Kouno And H. Irie, *Cheminform.*2010, **25**
16 R. Singh, G. C. Singh and S. K. Ghosh, *Eur. J. Org. Chem.*, 2007, **2007**, 5376–5385.
17 M. Peng, H. Li, R. Long, S. Shi, H. Zhou and S. Yang, *Molecules*, 2018, **23**, 7
18 Y. Gao, Y. Tang, L. Gao, Y. Niu, R. Gao, X. Chen, Y. Hao and S. Wang, *Anal. Chim. Acta*, 2021, **1161**, 338475.
19 B. Sun, X. Hou, D. Li, Y. Gou, F. Hu, W. Li and X. Shi, *J. Electrochem. Soc.*, 2019, **166**, B1644.
20 Y. Hu, W. Huang, T. Yukui, Q. Xia and M. Tian, *New J Chem*, 2017, **41**
21 M. Kocúrik, J. Bartáček, J. Svoboda, Z. Kolská, J. Chýlková and M. Sedlák, *Polymer*, 2022, **256**, 125189.
22 T. Sajini and B. Mathew, *Talanta Open*, 2021, **4**, 100072.
23 N. Maier and W. Lindner, *Anal. Bioanal. Chem.*, 2007, **389**, 377–97.
24 E. N. Ndunda, *J. Mol. Recognit.*, 2020, **33**, e2855.
25 B. Okutucu and N. Pazarlioglu, *Prep. Biochem. Biotechnol.*, 2010, **40**, 366–76.
26 J. Feher, in *Quantitative Human Physiology (Second Edition)*, ed. J. Feher, Academic Press, Boston, 2017, pp. 853–869.
27 M. Daoud Attieh, Y. Zhao, A. Elkak, A. Falcimaigne-Cordin and K. Haupt, *Angew. Chem. Int. Ed.*, 2017, **56**, 3339–3343.
28 B. E. Obi, in *Polymeric Foams Structure-Property-Performance*, ed. B. E. Obi, William Andrew Publishing, Oxford, 2018, pp. 17–40.
29 V. D. Salian, C. J. White and M. E. Byrne, *React. Funct. Polym.*, 2014, **78**, 38–46.
30 Y. Shen, H. Tang and S. Ding, *Prog. Polym. Sci.*, 2004, **29**, 1053–1078.
31 A. B. Asha, S. Srinivas, X. Hao and R. Narain, in *Smart Polymers and their Applications (Second Edition)*, eds. M. R. Aguilar and J. San Román, Woodhead Publishing, 2019, pp. 155–189.
32 V. D. Salian, A. D. Vaughan and M. E. Byrne, *J. Mol. Recognit.*, 2012, **25**, 361–369.
33 N. Truong Phuoc, G. Jones, K. Bradford, D. Konkolewicz and A. Anastasaki, *Nat. Rev. Chem.*, 2021, **5**
34 S. Perrier, *Macromolecules*, 2017, **50**, 7433–7447.
35 H. R. Lamontagne and B. H. Lessard, *ACS Appl. Polym. Mater.*, 2020, **2**, 5327–5344.
36 B. Fairbanks, T. Gunatillake and L. Meagher, *Adv. Drug Deliv. Rev.*

37 X. Zhao, W. Pei, R. Guo and X. Li, *Front. Chem.*
38 F. Deng, X.-B. Luo, L. Ding and S.-L. Luo, in *Nanomaterials for the Removal of Pollutants and Resource Reutilization*, eds. X. Luo and F. Deng, Elsevier, 2019, pp. 149–178.
39 M. D. Ariani, A. Zuhrotun, P. Manesiotis and A. N. Hasanah, *Polymers*, 2022, **14**, 1389.
40 A. Pardo, T. Josse, L. Mespouille, B. Blankert, P. Dubois and P. Duez, *Phytochem. Anal.*, 2017, **28**, 289–296.
41 L. Lajoie, A.-S. Fabiano-Tixier and F. Chemat, *Pharmaceuticals*, 2022, **15**,12
42 H. Wang, Y. Liu, S. Yao and P. Zhu, *Food Chem.*, 2018, **240**, 1262–1267.
43 C. Dong, H. Shi, Y. Han, Y. Yang, R. Wang and J. Men, *Eur. Polym. J.*, 2021, **145**, 110231.
44 M. D. Ariani, A. Zuhrotun, P. Manesiotis and A. N. Hasanah, *Polym. Adv. Technol.*, 2024, **35**, e6201.
45 X. Wang, Y. Feng, H. Chen, Y. Qi, J. Yang, S. Cong, Y. She and X. Cao, *Microchem. J.*, 2023, **185**, 108271.
46 J. M. Asua, *Prog. Polym. Sci.*, 2002, **27**, 1283–1346.
47 A. Poma, A. P. F. Turner and S. A. Piletsky, *Trends Biotechnol.*, 2010, **28**, 629–637.
48 S. Roy, S. Nagabooshanam, N. Chauhan, A. Mathur, S. Wadhwa, U. Jain and J. Davis, in *Multifaceted Bio-sensing Technology*, eds. L. Singh, D. Mahapatra and S. Kumar, Academic Press, 2023, vol. 4, pp. 111–134.
49 Y. Yang and X. Shen, *Molecules*, 2022, **27**, 7355.
50 X. Liu, W. Zhang and Z. Chen, *J. Sep. Sci.*, 2015, **38**, 4233–4239.
51 G. Zhao, J. Liu, M. Liu, X. Han, Y. Peng, X. Tian, J. Liu and S. Zhang, *Appl. Sci.*, 2020, **10**, 8
52 Y. Cheng, J. Nie, H. Liu, L. Kuang and G. Xu, *J. Chromatogr. A*, 2020, **1630**, 461531.
53 G. P. González, P. F. Hernando and J. S. D. Alegría, *Pap. Present. 2nd Int. Symp. Sep. Charact. Nat. Synth. Macromol.*, 2006, **557**, 179–183.
54 B. Jia, F. Feng, X. Wang, Y. Song and F. Zhang, *J. Future Foods*, 2024, **4**, 1–20.
55 J. Gong, Z. Jin, H. Chen, J. He, Y. Zhang and X. Yang, *Adv. Drug Deliv. Rev.*, 2023, **196**, 114791.
56 V. Pakade, S. Lindahl, L. Chimuka and C. Turner, *J. Chromatogr. A*, 2012, **1230**, 15–23.
57 S. Qwane, P. Mdluli and L. Madikizela, *South Afr. J. Chem. Suid-Afr. Tydskr. Vir Chem.*, 2020, **73**
58 M. Dogan, A. U. Dogan, F. I. Yesilyurt, D. Alaygut, I. Buckner and D. E. Wurster, *Clays Clay Miner.*, 2007, **55**, 534–541.
59 A. Mpupa, M. Dinc, B. Mizaikoff and P. Nomngongo, *Processes*, 2021, **9**, 186.
60 W. Sroysee, S. Chunta, M. Amatatongchai and P. A. Lieberzeit, *Phys. Med.*, 2019, **7**, 100016.
61 Y. Gong, X. Chen and W. Wu, *Adv. Sample Prep.*, 2024, **11**, 100122.
62 Z. Baker and S. Sardari, *Iran. Biomed. J.*, 2021, **25**, 68–77.
63 S. Villarreal, K. Vargas, L. Díaz de León-Martínez and R. Flores-Ramírez, *Environ. Sci. Pollut. Res.*, 2022, **29**
64 X. Ma, H. Lin, J. Zhang, X. Zhou, J. Han, Y. She, C. Qiu, Q. He, J. Wang and T. Rabah, *Green Chem. Lett. Rev.*, 2018, **11**, 513–522.
65 Q. Jia, Y. Ma, Y. Peng, Y. Liu and W. Zhang, *Chem. Eng. J.*, 2018, **342**, 293–303.
66 Abdullah, E. Alveroglu, A. Balouch, S. Khan, A. M. Mahar, M. S. Jagirani and A. H. Pato, *Microchem. J.*, 2021, **162**, 105849.
67 M. Meng and M. He, *Sep. Sci. Technol.*, 2016, **51**
68 R. Di, Y. Zhang, Z. Wu, W. Liu and C. Yang, *J. Mol. Liq.*, 2020, **302**, 112523.
69 D.-D. Wang, D. Gao, W.-J. Xu, F. Li, M.-N. Yin, Q.-F. Fu and Z.-N. Xia, *Talanta*, 2018, **184**, 307–315.
70 Y. Wan, M. Wang, Q. Fu, L. Wang, D. Wang, K. Zhang, Z. Xia and D. Gao, *J. Chromatogr. B*, 2018, **1097–1098**, 1–9.
71 S. Masumoto, Y. Nakamura and J. Haginaka, *J. Pharm. Biomed. Anal.*, 2021, **205**, 114294.
72 D. Wang, X. Luo, M. Wang, K. Zhou and Z. Xia, *J. Chromatogr. B*, 2020, **1156**, 122307.
73 K.-H. Liu, H.-Y. Lin, J. L. Thomas, Y.-P. Shih, Z.-Y. Yang, J.-T. Chen and M.-H. Lee, *J. Ginseng Res.*, 2022, **46**, 621–627.
74 J.-W. Zhang, L. Tan, Y.-Z. Zhang, G.-C. Zheng, Z.-N. Xia, C.-Z. Wang, L.-D. Zhou, Q.-H. Zhang and C.-S. Yuan, *J. Chromatogr. B*, 2019, **1104**, 205–211.
75 K. Hroboňová, A. Machyňáková and J. Čižmárik, *J. Chromatogr. A*, 2018, **1539**, 93–102.

76 S. Eidi, M. Iranshahi, A. Mohammadinejad, M. S. Mohsenzadeh, F. Farhadi and S. A. Mohajeri, *J. Chromatogr. B*, 2020, **1138**, 121943.
77 A. Machyňáková, I. Lhotská, K. Hroboňová and D. Šatínský, *J. Pharm. Biomed. Anal.*, 2017, **145**, 144–150.
78 C. Gomes, G. Sadoyan, R. C. S. Dias and M. R. P. F. N. Costa, *Processes*,2017 **5**, 4
79 M. Brenes, F. J. Hidalgo, A. García, J. J. Rios, P. García, R. Zamora and A. Garrido, *J. Am. Oil Chem. Soc.*, 2000, **77**, 715–720.
80 . Wikul, T. Damsud, K. Kataoka and P. Phuwapraisirisan, *Bioorg. Med. Chem. Lett.*, 2012, **22**, 5215–5217.
81 B. Hwang, J. Lee, Q.-H. Liu, E.-R. Woo and D. G. Lee, *Molecules*, 2010, **15**, 3507–3516.
82 T. Holmbom, M. Reunanen and P. Fardim, *Holzforschung*, 2008, **62**, 417–422.
83 M. Rautio, A. Sipponen, J. Lohi, K. Lounatmaa, P. Koukila-Kähkölä and K. Laitinen, *Eur. J. Clin. Microbiol. Infect. Dis.*, 2012, **31**, 1783–1789.
84 V. Srivastava, M. Singh, R. Malasoni, K. Shanker, R. K. Verma, M. M. Gupta, A. K. Gupta and S. P. S. Khanuja, *J. Sep. Sci.*, 2008, **31 1**, 47–55.
85 S. Willför, P. Eklund, R. Sjöholm, M. Reunanen, R. Sillanpää, S. von Schoultz, J. Hemming, L. Nisula and B. Holmbom, 2005, **59**, 413–417.
86 B. Chatterjee, D. Mondal and S. Bera, *Beilstein J. Org. Chem.*, 2024, **20**, 1376–1395.
87 L. Panzella, M. DellaGreca and L. Longobardo, *ChemistrySelect*, 2018, **3**, 10637–10640.
88 A. Hosoda, E. Nomura, K. Mizuno and H. Taniguchi, *J. Org. Chem.*, 2001, **66**, 7199–7201.

Appendices

Appendix 1. Overlaid chromatograms from multi-solvent sequential hot extraction, with Pinoresinol 1 marked with a black arrow.

Appendix 2. Calibration method LOD and LOQ values for all measured wavelengths

BMB-Al **5** S/N, LOD, and LOQ determination

λ (nm)	Noise band	Noise	S/N	LOD_m (ug)	LOQ_m (ug)	LOD_h (mAU)	LOQ_h (mAU)
280	0.030	0.015	286.7	0.0002	0.0006	0.06	0.18
254	0.030	0.015	80.0	0.0002	0.0006	0.02	0.05
230	0.075	0.038	128.0	0.0005	0.0016	0.07	0.21
210	0.150	0.075	92.0	0.0011	0.0032	0.10	0.30

BMB-A **3** S/N, LOD, and LOQ determination

λ (nm)	Noise band	Noise	S/N	LOD_m (ug)	LOQ_m (ug)	LOD_h (mAU)	LOQ_h (mAU)
280	0.030	0.015	166.7	0.0002	0.0006	0.03	0.10
254	0.030	0.015	340.0	0.0002	0.0006	0.07	0.21
230	0.075	0.038	136.0	0.0005	0.0015	0.07	0.21
210	0.150	0.075	161.3	0.0010	0.0031	0.17	0.50

BMB-OH **4** S/N, LOD, and LOQ determination

λ (nm)	Noise band	Noise	S/N	LOD_m (ug)	LOQ_m (ug)	LOD_h (mAU)	LOQ_h (mAU)
280	0.030	0.015	100.0	0.0002	0.0006	0.02	0.06
254	0.030	0.015	42.7	0.0002	0.0006	0.01	0.02
230	0.075	0.038	128.0	0.0005	0.0014	0.06	0.18
210	0.150	0.075	221.3	0.0010	0.0029	0.21	0.64

Appendix 3. Example of overlaid chromatograms (230 nm) of one calibration series.

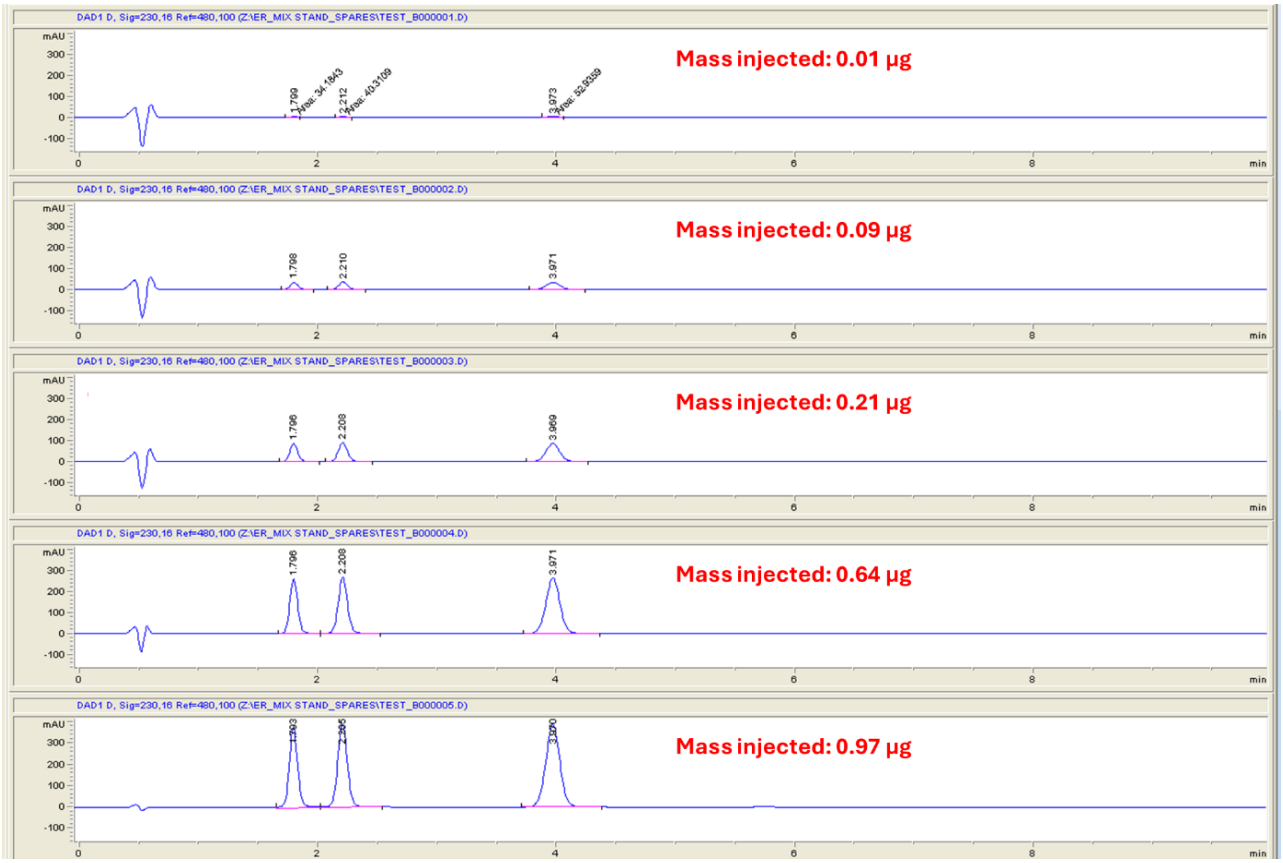

Appendix 4. Example of a calibration series peak areas fitted against injected mass with the regression analysis

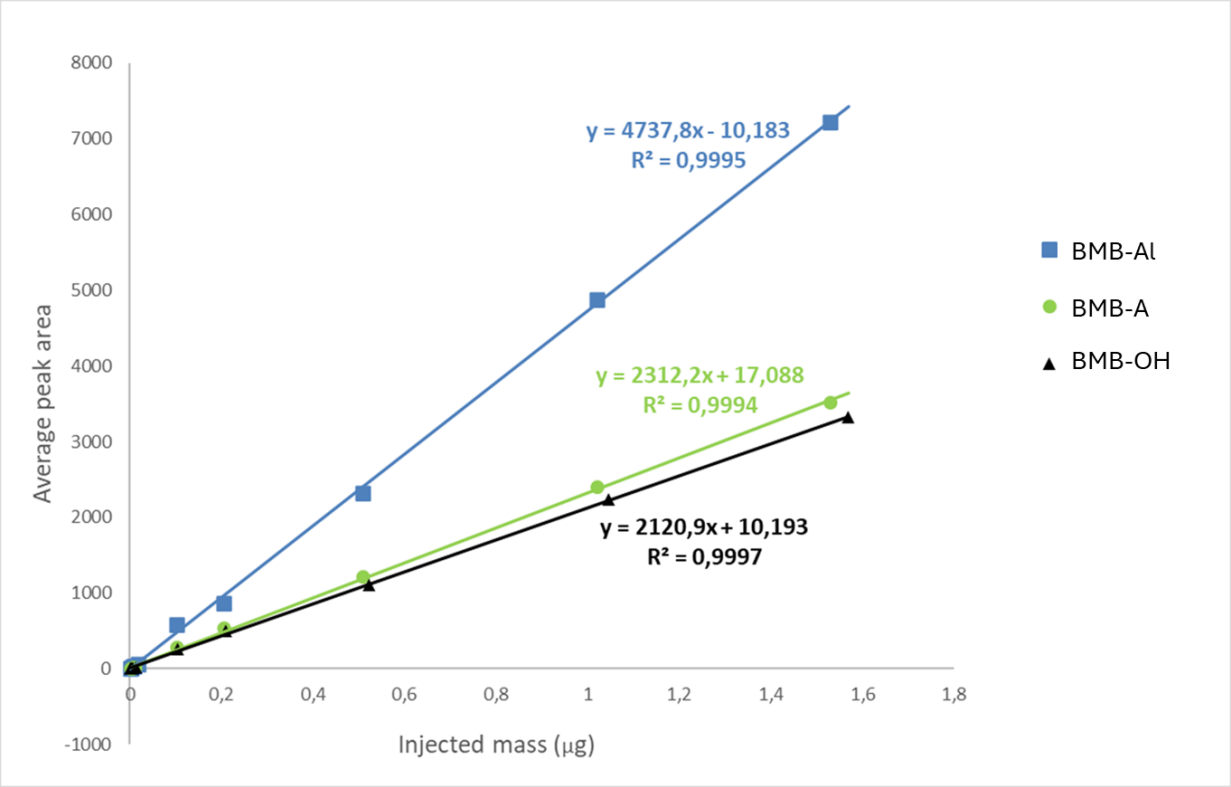

Appendix 5. Chromatograms (230 nm) of the Cannizzaro products from homogeneous and heterogeneous reaction conditions

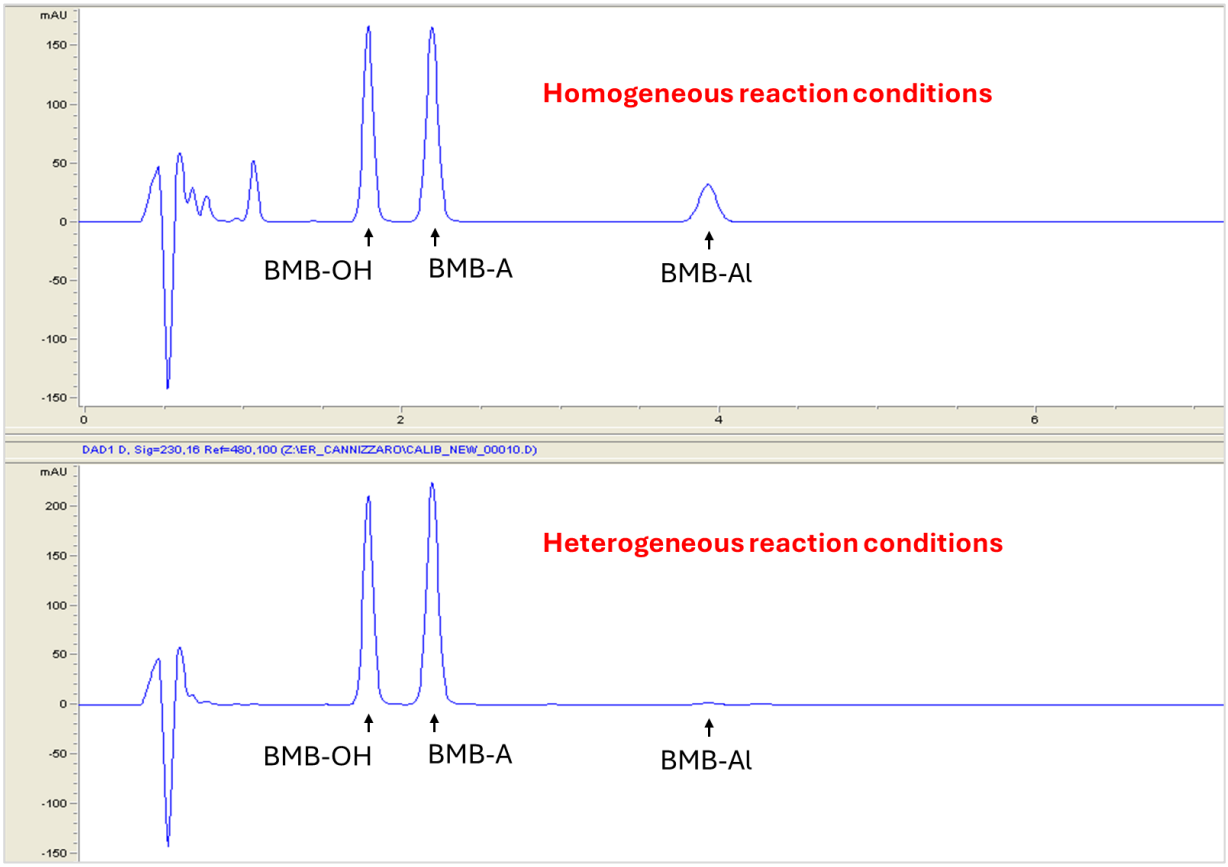

Appendix 6. Chromatographs of crude and recrystallized 4-Acetoxyferulic acid and the mother liquor of the recrystallization

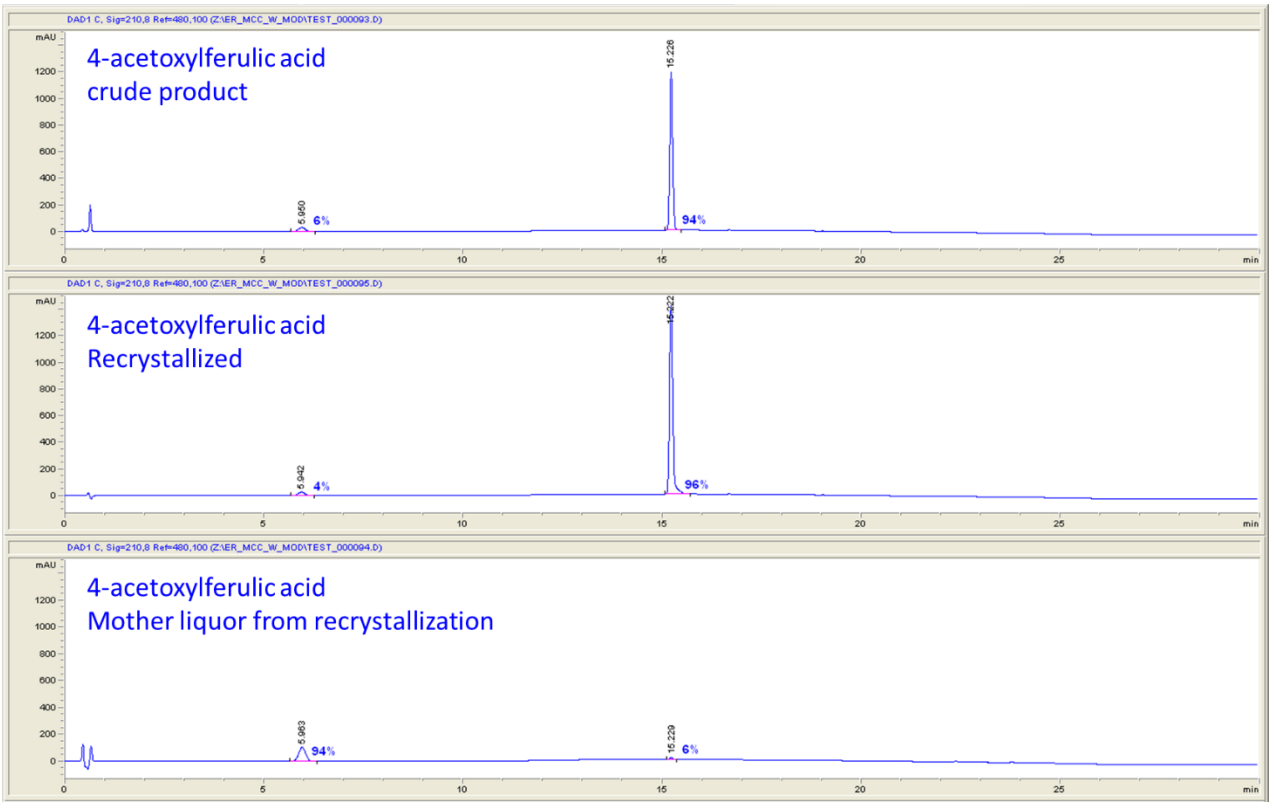

Appendix 7. Overlaid chromatograms of the reduction of 4-Acetylferuloyl chloride 12 (red arrow) to produce 4-Acetoxyconiferyl alcohol 13 (black arrow).